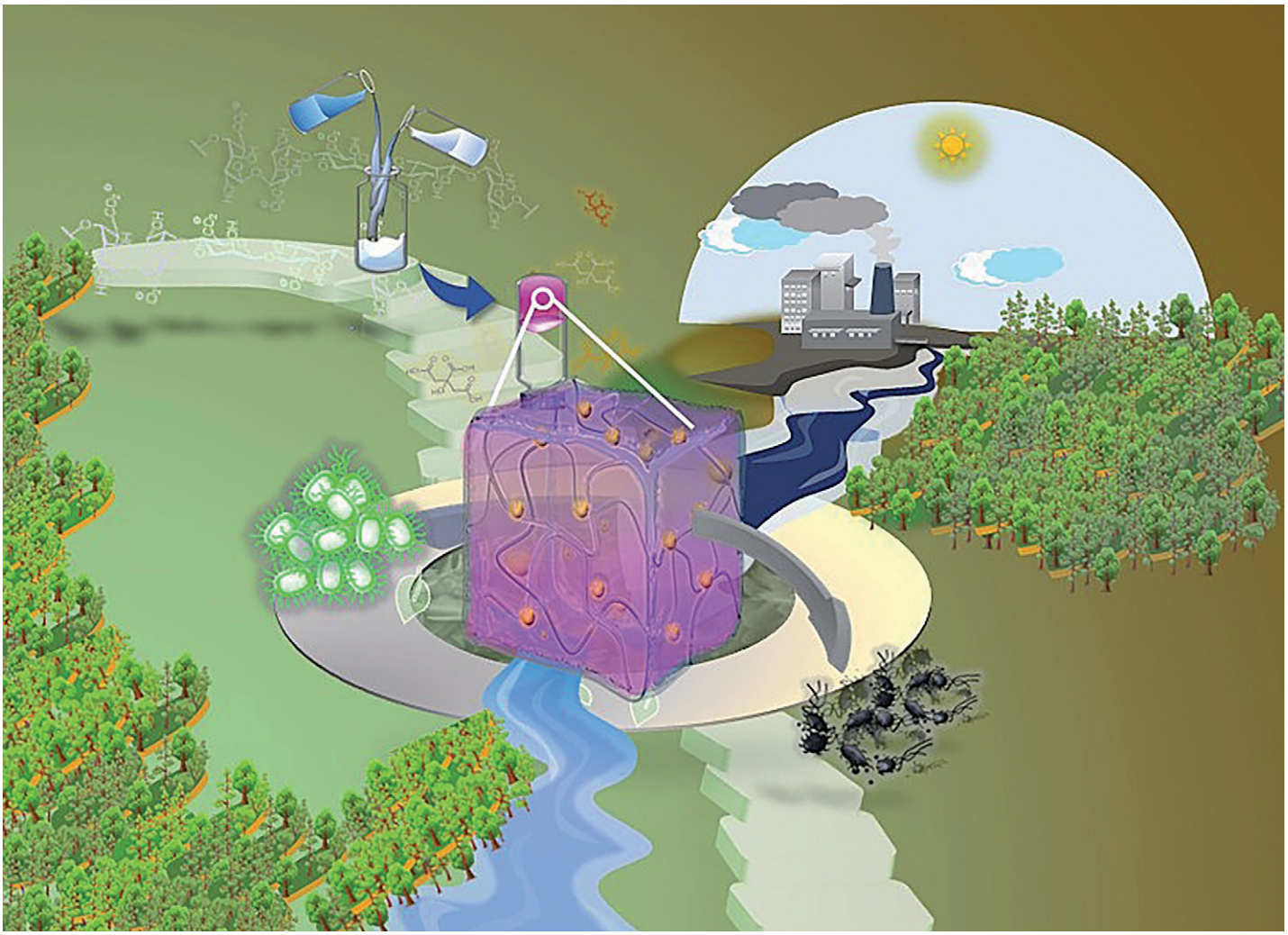

Showcasing research from Dr. Chandan Maity's (Organic) Material Science and Engineering Laboratory at Centre of Nanobiotechnology (CNBT), Vellore Institute of Technology, Vellore Campus, Tamil Nadu, India.

Facile room-temperature one-pot synthesis of a gold nanoparticle-embedded hydrogel for recyclable dye degradation and antimicrobial applications

This study presents a simple, equipment-free one-pot synthesis of gold nanoparticle–embedded alginate hydrogels at room temperature, using citric acid as both crosslinker and reducing agent. *In situ* formed gold nanoparticles display strong catalytic activity, enabling rapid degradation of Congo red and methylene blue with high reusability. The hydrogel also effectively treats real textile wastewater. Additionally, it exhibits broad-spectrum antibacterial activity via ROS-mediated membrane disruption and controlled nanoparticle release, highlighting promise for environmental remediation and biomedical applications in resource-limited settings and scalable sustainable material design for future technologies.

Image reproduced by permission of Damini Jagankar and Chandan Maity from *Environ. Sci.: Nano*, 2026, **13**, 257.

As featured in:

See Chandan Maity *et al.*, *Environ. Sci.: Nano*, 2026, **13**, 861.

ROYAL SOCIETY OF CHEMISTRY

rsc.li/es-nano

Registered charity number: 207890

Environmental Science Nano

ROYAL SOCIETY OF CHEMISTRY

PAPER

View Article Online
View Journal | View Issue

Check for updates

Cite this: *Environ. Sci.: Nano*, 2026, 13, 861

Facile room-temperature one-pot synthesis of a gold nanoparticle-embedded hydrogel for recyclable dye degradation and antimicrobial applications

Damini Jagankar,[ab] Geethika Manohar,[b] Priyanka Srivastava [b] and Chandan Maity *[ab]

Received 4th August 2025,
Accepted 8th December 2025

DOI: 10.1039/d5en00722d

rsc.li/es-nano

This work reports a sustainable and equipment-free one-pot strategy for the synthesis of gold nanoparticles (Au NPs) embedded within a hydrogel matrix at room temperature. In this method, Au NPs are formed *in situ* through simple mixing of aqueous sodium alginate (Alg, 3 wt%), citric acid (CA, 0.5 M), and chloroauric acid (0.5 mM), where CA serves a dual role as both crosslinker and a reducing agent. The resulting hydrogel exhibits excellent catalytic activity toward the reductive degradation of organic dyes, achieving rapid decolorization efficiencies of 91% for Congo red and 97% for methylene blue within 5 min in the presence of sodium borohydride while maintaining reusability over five cycles. Besides, the material also effectively degrades real wastewater samples from the textile industry, highlighting its potential for sustainable wastewater treatment applications. Additionally, the material exhibits potent antibacterial activity against *Staphylococcus aureus*, *Escherichia coli*, and *Acinetobacter baumannii*. This activity is attributed to reactive oxygen species (ROS)-mediated membrane disruption, and the sustained release of Au NPs from the hydrogel matrix. This simple one-pot synthesis strategy highlights significant potential for biomedical application and environmental remediation, especially in resource-limited settings.

Environmental significance

This study presents a simple, one-pot, equipment-free synthesis of gold nanoparticle (Au NP)-embedded hydrogel material, offering a green and scalable approach to environmental remediation and antimicrobial applications. The use of biocompatible organic citric acid functioning both as a crosslinker for the alginate biopolymer chain and reducing agent for *in situ* preparation of Au NPs eliminates the need for toxic chemicals, high temperatures, or specialized equipment. The resulting composite exhibits rapid and efficient catalytic degradation of synthetic dyes and real textile wastewater alongside strong antibacterial activity against key pathogens. Its reusability, effectiveness in real-world conditions, and eco-friendly synthesis make this material highly suitable for wastewater treatment in low-resource or decentralized settings, contributing to sustainable environmental and public health solutions.

1. Introduction

Environmental contamination is a critical issue of the modern world. Emerging environmental pollutants such as organic dyes, pesticides, herbicides, pharmaceuticals, heavy metals, and microplastics are increasingly polluting water sources through direct industrial discharge and/or *via* improper disposal practices. Among various pollutants, organic dyes are of particular concern, as they are extensively discharged by textile, plastic, printing, cosmetic, and pharmaceutical industries. These dyes are often toxic, non-biodegradable, and potentially carcinogenic, posing serious risks to aquatic ecosystems and human health through bioaccumulation.[1,2] Conventional physical, chemical, and biological pollutant removal methods are often effective but face challenges such as high cost, use of toxic chemicals, and limited reusability.[3–5] Therefore, the development of simple, cost-effective, and environmentally benign approaches for efficient dye degradation remains an urgent challenge, crucial for advancing sustainable water reclamation and reuse to meet growing global water demand.

On the other hand, microbial contaminants such as bacteria, viruses, and fungi pose a major threat to human health that can cause extensive social and economic problems.[6] Infectious pathogens increase the risk of tissue

[a] *(Organic)Material Science and Engineering Laboratory, Centre for Nanobiotechnology (CNBT), Vellore Institute of Technology (VIT), India.* https://sites.google.com/view/omates-lab/home

[b] *Centre for Nanobiotechnology (CNBT), Vellore Institute of Technology (VIT), Vellore Campus, Tamil Nadu-632014, India. E-mail: chandanmaitylab@gmail.com, chandan.maity@vit.ac.in*

morbidity and sepsis, resulting in prolonged recovery time and inflating the mortality rate. Besides, misuse of conventional antibiotics has already led to emergence of multidrug-resistant strains, decreasing the efficacy of current therapeutic treatments.[7,8] Therefore, there is a continuous need and urgency for developing newer antimicrobial materials.

Development of multifunctional materials capable of degrading organic dyes and exhibiting antimicrobial activity is of critical importance. Towards this, composite materials that integrate two or more functional components could provide an amenable solution addressing the dual functionality.[9–12] Among these, metal-based nanoparticle (NP)-incorporated hydrogels have received significant attention due to the synergistic properties between the unique properties of NPs and the structural advantages of hydrogels. Nanoparticles possess distinctive physicochemical features, including high surface area, tuneable surface chemistry, and reactivity, and can exhibit catalytic and antimicrobial activities. However, their tendency to aggregate or lose stability in aqueous environments often limits their performance. Hydrogels, on the other hand, are three-dimensional, porous molecular networks capable of retaining substantial amounts of water, providing a hydrated and biocompatible microenvironment. The incorporation of NPs into hydrogel matrices effectively overcomes their instability by offering spatial confinement and preventing aggregation. This integration yields nanocomposite hydrogels with enhanced stability, reusability, and functional efficiency, making them highly suitable for diverse applications such as catalytic dye degradation and antimicrobial treatments.[13,14]

In recent years, a wide range of nanoparticles, particularly metal and metal oxide NPs, have been incorporated into polymer-based hydrogel frameworks to develop multifunctional composite materials. Among these, gold nanoparticles (Au NPs) have attracted significant attention due to their excellent biocompatibility, high surface-to-volume ratio, tuneable optical properties, and remarkable catalytic activity.[15–17] However, the unique properties of Au NPs are dependent on their nanoscale dimensions; therefore, precise control over their size and size distribution is crucial for achieving effective performance in applications.[18,19] Well-defined Au NP morphologies can be achieved through *in situ* synthesis *via* chemical reduction of gold precursors such as tetrachloroauric acid ($HAuCl_4$), involving nucleation followed by controlled growth.[15,20] However, the majority of Au NP synthesis methods require high temperature and use of a light source, high-power ultrasound or sophisticated instruments. While thiol-based ligands enable Au NP synthesis at ambient temperature, the procedures still depend on the use of toxic chemicals and organic solvents and the presence of specific ligand precursors.[21,22] In an eco-friendly and cost-effective way, plant-based extracts have been employed as a reducing agent and stabilizer for the preparation of Au NPs.[23,24] However, limited understanding of the roles of specific extracts for chemical reaction(s), unavailability of standardized procedures, and incorporation of unwanted plant compounds into the final product are the limitations of this approach. Therefore, development of an environment-friendly approach for controlled formation of Au NPs under ambient conditions without using toxic substances is highly desirable for biomedical applications and environmental remediation. In this regard, three-dimensional hydrogel networks offer distinct advantages for the preparation of Au NPs over conventional non-aqueous systems. Their highly porous, biocompatible, and hydrated nature facilitates the diffusion of small molecules, and the space within hydrogel matrices can serve as confined nanoreactors for the nucleation and growth of nanocrystals.[16,25,26]

Among various hydrogel systems, biomaterial-derived hydrogels such as carboxymethylcellulose, chitosan, and lignin are particularly attractive owing to their abundance, low cost, renewability, and environmental friendliness.[25,27–29] Incorporating Au NPs within such hydrogel matrices synergistically combines the mechanical stability, responsiveness, and biocompatibility of the hydrogel with the unique catalytic, optical, and antimicrobial properties of Au NPs. Although several studies have reported Au NP–hydrogel composites for dye degradation and antimicrobial applications, many of these methods still rely on elevated temperatures, toxic solvents, or prolonged reaction times, underscoring the need for simpler, greener alternatives.[30,31]

Herein, we report an eco-friendly and facile *in situ* synthesis of Au NPs embedded within a sodium alginate–citric acid (Alg–CA) hydrogel matrix (Fig. 1a). The Alg–CA network provides a biocompatible platform that supports the nucleation and controlled growth of monodisperse Au NPs while preventing their aggregation. The synthesis is accomplished under ambient conditions through simple mixing of aqueous sodium alginate (Alg), citric acid (CA), and tetrachloroauric acid ($HAuCl_4$) (Fig. 1b) without requiring external reducing agents, elevated temperatures, or specialized equipment.

It is worth mentioning that we have recently demonstrated the preparation of silver-based nanoparticles within a hydrazone-crosslinked hydrogel matrix derived from aldehyde-functionalized alginate and guanidine-based hydrazides.[32] The present approach employs unmodified alginate and citric acid, enabling a truly one-pot, green fabrication process. The resulting Au NPs/Alg–CA hydrogel exhibits excellent catalytic efficiency for the degradation of organic dyes, tested with individual, mixed, and real wastewater samples, while maintaining excellent recyclability. Furthermore, the composite displays potent antimicrobial activity, effectively inhibiting microbial growth. This multifunctional, sustainable material thus holds significant promise for applications in environmental remediation and healthcare.

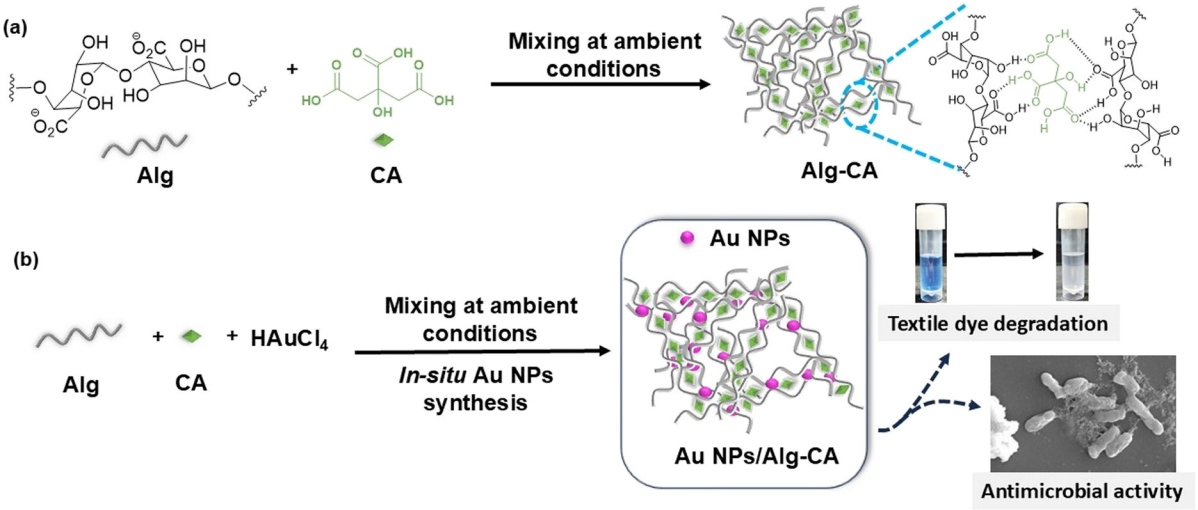

Fig. 1 Preparation of an Au NP-integrated alginate hydrogel material. (a) A schematic presentation of alginate hydrogel material (Alg–CA) preparation by mixing aqueous solutions of sodium alginate and an organic acid crosslinker. (b) Schematic representation of *in situ* preparation of the Au NPs/Alg–CA composite by mixing aqueous solutions of alginate, organic acid, and $HAuCl_4$ under ambient conditions. The resulting composite exhibits catalytic activity for organic dye degradation and demonstrates antimicrobial properties.

2. Materials and methods

2.1. Materials

All reagents and solvents were commercially available and used as received without further purification. Sodium alginate and tetrachloroauric acid trihydrate ($HAuCl_4{\cdot}3H_2O$) were obtained from Sisco Research Laboratories Pvt. Ltd. (India). Anhydrous citric acid (AR, ACS grade) was purchased from S D Fine-Chem Ltd. (India). Congo red (75%) was procured from SRL Pvt. Ltd. (India), and methylene blue (M. S. grade) from Nice Chemicals Pvt. Ltd. (India). Sodium borohydride ($NaBH_4$, 96%) was purchased from Sigma-Aldrich (India).

Bacterial strains, including *Staphylococcus aureus* (MTCC 96), *Escherichia coli* (MTCC 739), and *Acinetobacter baumannii* (MTCC 1425), were obtained from Microbial Type Culture Collection (MTCC, CSIR-Institute of Microbial Technology, Chandigarh, India). Mueller–Hinton agar, Mueller–Hinton broth, and a dialysis membrane (MWCO 60) were purchased from HiMedia Laboratories Pvt. Ltd. (India). Fluorescent and cell viability reagents, 2′,7′-dichlorofluorescein diacetate (DCFH-DA) and 3-(4,5-dimethylthiazol-2-yl)-2,5-diphenyltetrazolium bromide (MTT) were obtained from Sigma-Aldrich (USA). Inorganic salts, including potassium chloride, sodium bicarbonate, potassium dihydrogen phosphate, ammonium carbonate, and magnesium chloride, were purchased from SRL Pvt. Ltd. (India).

2.2. Instrumentation

The optical properties of the Au NP-incorporated hydrogel were analysed using a UV-visible spectrophotometer (JASCO V-670 PC). Absorption spectra were recorded over the wavelength range of 250–600 nm. Functional groups present in the hydrogel nanocomposite were investigated by Fourier-transform infrared (FTIR) spectroscopy (IR Affinity-1, Shimadzu, Japan). For FTIR measurements, samples were first stored at 4 °C for 24 h and subsequently freeze-dried using a lyophilizer. Spectra were recorded in the range of 500–4000 cm^{-1}. Powder X-ray diffraction (p-XRD) analysis was performed using a Bruker D8 Advance diffractometer (Analytical Xpert, Germany/Netherlands) to confirm the formation of Au NPs within the hydrogel network. Thin films of the hydrogel were prepared on glass coverslips and air-dried prior to measurement. Morphological and elemental analyses were conducted using field emission scanning electron microscopy (FESEM, Thermo Fisher FEI Quanta 250 FEG) coupled with energy-dispersive X-ray (EDX) spectroscopy. High-resolution transmission electron microscopy (HRTEM, FEI Titan Themis 60–300 kV, Thermo Fisher) was employed to obtain detailed micrographs of the hydrogel nanocomposite.

2.3. Synthesis of Alg–CA

The alginate–citric acid (Alg–CA) hydrogel was prepared under ambient conditions by simply mixing an aqueous solution of unmodified sodium alginate (Alg, 3.0 wt%) and a solution of citric acid (CA, 0.5 M). Gelation was indicated by the formation of a homogeneous, opaque hydrogel, which was confirmed qualitatively using the vial inversion test.

2.4. Synthesis of Au NPs/Alg–CA

The Au NP-incorporated Alg–CA hydrogel (Au NPs/Alg–CA) was prepared under ambient conditions by mixing aqueous solutions of Alg (3 wt%), CA (0.5 M), and tetrachloroauric acid ($HAuCl_4$, 0.5×10^{-3} M) at room temperature. Gelation was observed as the mixture turned into a homogeneous, opaque hydrogel, which was confirmed using the vial

inversion test. A characteristic pink coloration developed within 5 h, indicative of Au NP formation, and remained stable over 24 h.

2.5. Catalytic degradation of organic dyes

The catalytic activity of the Au NPs/Alg–CA hydrogel was evaluated using Congo red (CR) and methylene blue (MB) as model organic dyes. In a typical experiment, 2.0 mL of the hydrogel composite was mixed with an aqueous solution of the dye and freshly prepared $NaBH_4$ (10.0 mM) under ambient conditions with gentle shaking. Aliquots were withdrawn at predetermined time intervals, and the progress of the dye degradation was monitored by recording the UV-visible absorption spectra. Control experiments were performed under identical conditions in the absence of the hydrogel composite.

2.6. Kinetic analysis of dye degradation

For the catalytic degradation experiments, $NaBH_4$ (10.0 mM) was added to aqueous solutions of CR, MB, their mixture or wastewater. The decolorization of the dyes was monitored spectrophotometrically, and the reaction kinetics were evaluated using the following equation:

$$\ln\left(\frac{A_t}{A_0}\right) = -kt$$

where k = pseudo-1st-order rate constant, t = reaction time, A_t = absorbance of the dye at time t, and A_0 = absorbance of the dye at time $t = 0$.

2.7. Quantitative analysis of dye degradation

The degradation efficiency of CR and MB was calculated using the following formula:

$$\%\ \text{degradation} = \frac{A_0 - A_t}{A_0} \times 100$$

where A_0 = the initial absorbance of dye solution before treatment and A_t = the absorbance of the treated solution obtained at a specified time after degradation.

2.8. *In vitro* release of Au NPs

The release of Au NPs from the Au NPs/Alg–CA hydrogel was evaluated using a dialysis membrane. Approximately 1.0 g of the hydrogel sample was placed inside a dialysis bag, which was suspended in 300 mL of simulated salivary fluid (pH 6.8) and stirred at 300 rpm at 37 °C ± 0.5 °C.[33] Aliquots of 3 mL were withdrawn from the dissolution medium at 24 h intervals. To maintain sink conditions, the withdrawn volume was immediately replaced with an equal volume of fresh simulated salivary fluid (pH 6.8). The concentration of released Au NPs was quantified using atomic absorption spectroscopy (Perkin Elmer AAnalyst 400) at 243 nm. The cumulative release of Au NPs from the hydrogel was calculated using the following equation:

$$\%\ \text{particle release} = \left(\frac{Q_t}{Q_i}\right) \times 100$$

where Q_i and Q_t are the initial amounts of Au NPs entrapped in the Au NPs/Alg–CA and the released amount of gold nanoparticles at different time intervals.

2.9. Antibacterial activity

The antibacterial activity of the Au NPs/Alg–CA hydrogel and the control Alg–CA hydrogel (without Au NPs) was evaluated using the agar well diffusion and broth microdilution methods.

Agar well diffusion assay. A 100 μL inoculum of *Escherichia coli*, *Staphylococcus aureus*, or *Acinetobacter baumannii* was uniformly spread onto Mueller–Hinton agar (MHA) plates to form a bacterial lawn. Wells (5 mm diameter) were aseptically punched into the agar, and 100 μL of either Au NPs/Alg–CA or Alg–CA hydrogel was added to each well. The plates were incubated at 37 °C for 18–24 h, and the antibacterial activity was assessed by measuring the diameter of the inhibition zones (mm). All experiments were performed in duplicate, and results are reported as mean ± standard deviation (SD).

Minimum inhibitory concentration (MIC) determination. Following preliminary screening, the MIC of the Au NPs/Alg–CA hydrogel was determined using the broth microdilution method. The Au NPs/Alg–CA and Alg–CA samples were serially diluted twofold in Mueller–Hinton broth (MHB) to obtain final concentrations of 0.5, 0.25, 0.12, 0.06, 0.03, 0.015, 0.0075, 0.00375, 0.0018, 0.0009, and 0.0004 mg mL^{-1}. A bacterial suspension of *E. coli*, *S. aureus*, or *A. baumannii* (10^4 CFU mL^{-1}) was prepared in sterile MHB, and 50 μL of the suspension was added to each well of a 96 well microplate containing the diluted samples. Wells containing the bacterial inoculum without any antibacterial agent served as controls. The plates were incubated at 37 °C for 18 h, and bacterial growth was quantified by measuring the optical density at 600 nm (OD_{600}) using a UV-visible spectrophotometer (Thermo Scientific Evolution 220). The MIC was defined as the lowest sample concentration that completely inhibited visible bacterial growth. All experiments were conducted in triplicate, and percentage inhibition and bacterial growth were calculated from absorbance data.

2.10. Time-kill kinetics assay

The time-kill kinetics assay was performed to evaluate the rate of bacterial killing by the Au NPs/Alg–CA hydrogel, following standard protocols.[34] Individual colonies of *Escherichia coli*, *Staphylococcus aureus*, and *Acinetobacter baumannii* were isolated from overnight cultures and suspended in sterile normal saline to achieve a turbidity equivalent to a 0.5 McFarland standard.

The suspension was then adjusted to an inoculum size of approximately 1.0×10^6 CFU mL^{-1} in sterile broth and incubated at 37 °C. Aliquots (1 mL) of Au NPs/Alg–CA and Alg–CA (control) samples were prepared at their respective MIC concentrations and added to the bacterial suspensions. Tubes were incubated at 35 °C for 24 h, with one control tube containing no sample. At predetermined time intervals (0, 2, 4, 6, 8, and 24 h), 200 μL aliquots were withdrawn from each tube, and bacterial growth was monitored by measuring the absorbance at 630 nm using a UV-visible spectrophotometer (Thermo Scientific Evolution 220). All experiments were performed in triplicate, and a plot of absorbance *versus* time was used to determine the bacterial killing profile.

2.11. FESEM analysis of bacterial morphology

Morphological alterations in bacterial cell membranes before and after treatment with the Au NPs/Alg–CA and Alg–CA hydrogels were examined using field emission scanning electron microscopy (FESEM). Treated and untreated cultures of *Escherichia coli*, *Staphylococcus aureus*, and *Acinetobacter baumannii* were incubated overnight at 37 °C. Following incubation, the bacterial cells were harvested by centrifugation at 8000 rpm for 10 min, washed twice with sterile phosphate-buffered saline (PBS), and resuspended in the same buffer. Next, a drop of the bacterial suspension was placed on a clean glass slide to prepare a smear, which was heat-fixed and subsequently treated with 2.5% glutaraldehyde for 18 h at 4 °C for fixation. The samples were then dehydrated sequentially with graded ethanol solutions (30%, 60%, 70%, and 100%) and air-dried. The surface morphology of the fixed cells was analyzed using a field emission scanning electron microscope (Thermo Fisher FEI Quanta 250 FEG).

2.12. Intracellular reactive oxygen species assay

Intracellular reactive oxygen species (ROS) generation was quantified using 2′,7′-dichlorofluorescein diacetate ($DCFH_2$-DA). This non-fluorescent probe diffuses passively into cells, where it is deacetylated and subsequently oxidized by ROS to form the highly fluorescent compound 2′,7′-dichlorofluorescein (DCF).[35] A stock solution of $DCFH_2$-DA (10 mM) was prepared in dimethyl sulfoxide (DMSO) and diluted with phosphate-buffered saline (PBS) to obtain a 100 μM working solution.

Bacterial cells treated with Au NPs/Alg–CA and Alg–CA hydrogels were incubated overnight at 37 °C. After incubation, the cells were centrifuged, washed twice with PBS, and resuspended in 100 μM $DCFH_2$-DA solution. The suspensions were incubated in the dark for 30 min at room temperature, followed by centrifugation and washing with PBS to remove unbound dye. The fluorescence intensity of oxidized DCF was measured using a fluorescence spectrophotometer (Cary Eclipse, Model G9800A, Agilent Technologies, USA) at excitation and emission wavelengths of 492 nm and 523 nm, respectively.

2.13. Bacterial cell viability (MTT assay)

Bacterial cell viability was assessed using the 3-(4,5-dimethylthiazol-2-yl)-2,5-diphenyltetrazolium bromide (MTT) assay, following standard protocols.[36] The assay was employed to evaluate the antibacterial efficacy of the synthesized Au NPs/Alg–CA and Alg–CA formulations against *Escherichia coli*, *Staphylococcus aureus*, and *Acinetobacter baumannii*. Bacterial cultures were grown overnight in nutrient broth at 37 °C and adjusted to a 0.5 McFarland standard (approximately 1×10^8 CFU mL^{-1}). A 100 μL aliquot of the bacterial suspension was added to each well of a sterile 96 well microtiter plate, followed by 100 μL of the Au NPs/Alg–CA or Alg–CA formulations at various concentrations. The plates were incubated at 37 °C for 24 h. After incubation, 20 μL of MTT solution (5 mg mL^{-1} in PBS) was added to each well, and the plates were further incubated for 4 h to allow the reduction of MTT to insoluble formazan crystals by metabolically active cells. Subsequently, 100 μL of dimethyl sulfoxide (DMSO) was added to dissolve the formazan, and the absorbance was recorded at 570 nm using a UV-visible spectrophotometer (Thermo Scientific Evolution 220). The percentage of bacterial viability was calculated by comparing the absorbance values of treated and untreated samples. This assay provided a quantitative measure of bacterial metabolic activity and was used to determine the antibacterial potency of the formulations.

2.14. Statistical analysis

All experiments were performed in triplicate ($n = 3$), and the results are expressed as mean ± standard deviation (SD). Statistical analysis was carried out using GraphPad Prism 5 software. One-way analysis of variance (ANOVA) followed by Tukey's *post hoc* test was applied to evaluate the significance of differences between test samples and control groups. A p value <0.05 was considered statistically significant.

3. Results and discussion

3.1. Synthesis rationale

Environment-friendly, one-pot, and facile preparation of nanoparticle-integrated hydrogel materials under ambient conditions is based on the following considerations: (a) the hydrogel material should be synthesized under ambient conditions by simply mixing aqueous solutions of the precursors. (b) The hydrogel network would provide a favourable environment for the nucleation and growth of NPs, thereby regulating their size and morphology. (c) The formed NPs should remain well-dispersed and stable within the hydrogel matrix without agglomeration, eliminating the need for external stabilizers or specific ligands. (d) The integrated NPs and hydrogel network should exhibit synergistic properties that are not attainable from the individual components. (e) The overall preparation process should be facile and biocompatible, making the resulting material suitable for biomedical and environmental remediation applications.

3.2. Preparation of Alg–CA

Employing unmodified sodium alginate (Alg), hydrogel materials can be prepared with small organic molecules such as carboxylic acids and dimethyl sulfoxide.[37,38] Based on the guidelines and easy availability of the precursors, the Alg–CA hydrogel was prepared at room temperature from Alg and CA (Fig. 2a). Rheology measurement supported the viscoelastic properties of Alg–CA as the material showed frequency dependence from 0.1 to 100.0 rad s^{-1} with storage moduli (G') dominating loss moduli (G'') (Fig. 2b). The maximum G' value was recorded as 6.0 kPa at a strain of 1%. The strain sweep showed the linear viscoelastic region of Alg–CA, where G' was independent of the applied deformation (Fig. 2c). Fourier-transform infrared (FT-IR) absorption spectra of Alg–CA matched with Alg, albeit a slight blue shift for the stretching band for CO_2^- (1594 cm^{-1}) and the C–O stretching band (1175 cm^{-1}), suggesting involvement of hydrogen bonding (Fig. 2d). This observation is consistent with reported metal ion-free alginate hydrogel systems and can be attributed to ionic and hydrogen-bonding interactions between the –COOH and –OH groups of the alginate chains and those of the CA crosslinker.[37,39] In order to obtain morphological insight, field emission scanning electron microscopy (FESEM) images were recorded. A flower-like porous surface was observed for Alg–CA (Fig. 2e and S1). The energy-dispersive X-ray spectrometry (EDX) spectrum for Alg–CA revealed the presence of carbon, oxygen, and sodium (Fig. S2). It is worth mentioning that lower concentrations of CA or Alg did not provide the hydrogel material. Besides, hydrogelation was not observed in buffer solution (PBS buffer, 0.1 M) presumably due to disruption of ionic interactions between CA and Alg in the presence of salts in the buffer solution.

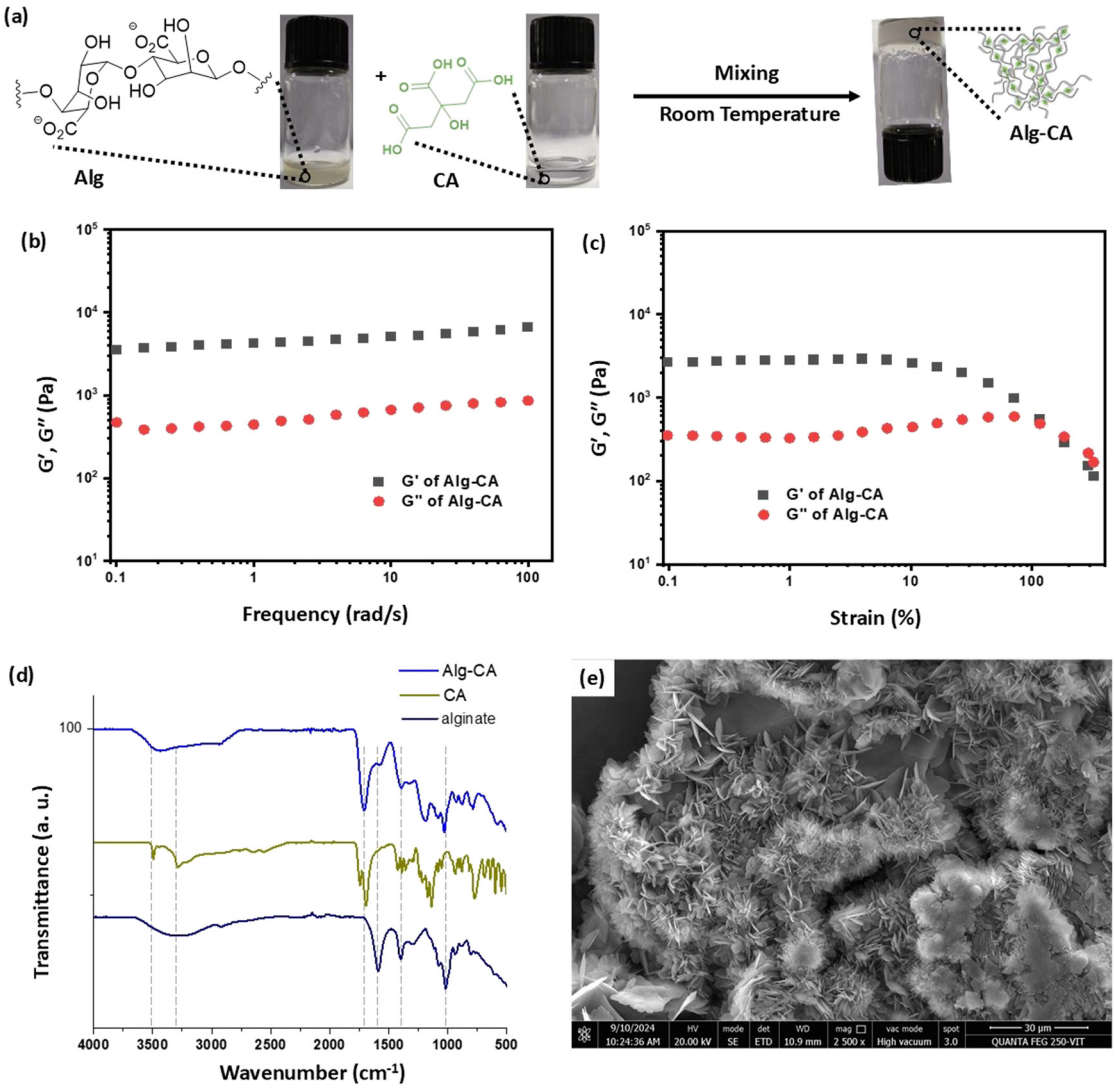

Fig. 2 Preparation of Alg–CA under ambient conditions. (a) A schematic for Alg–CA preparation by mixing sodium alginate (Alg) and citric acid (CA) at room temperature. (b and c) Rheology measurement for Alg–CA: (b) frequency sweep (performed at 0.1% strain) and (c) strain sweep (performed at 0.5 rad s^{-1} frequency). (d) Comparative IR spectra of Alg–CA (top), CA (middle) and Alg (bottom). (e) FESEM image of Alg–CA. Scale bar: 30 µm.

3.3. *In situ* preparation of Au NPs in Alg–CA

Having the Alg–CA preparation method under ambient conditions in hand, we envisioned that the Alg–CA hydrogel network could be employed as an efficient scaffold for the preparation of Au NPs as crosslinker CA could facilitate Au NP formation within the hydrogel network. In addition, the 3D network of the hydrogel material would prevent the aggregation of Au NPs.[40,41] It is worth noting that high temperature is generally required for the preparation of Au NPs using CA as the reducing agent and stabilizing agent. We prepared Au NPs/Alg–CA under ambient conditions by mixing aqueous solutions of Alg, CA, and $HAuCl_4$ (Fig. 3a). Formation of an opaque hydrogel was observed after mixing the precursors that gradually changed to a pink-coloured hydrogel in 5 h (Video S1).

Gradual change in the colour of the opaque hydrogel to pink indicated *in situ* formation of Au NPs within the hydrogel network, where the formation of the Alg–CA network is faster than the formation of Au NPs. The ultraviolet-visible (UV-vis) spectroscopy spectrum of Au NPs/Alg–CA showed an absorption maxima at 540 nm that was absent in the spectrum of only Alg–CA (Fig. 3b). This can be ascribed to the surface plasmon resonance (SPR) of Au NPs formed within the hydrogel network of Alg–CA and the SPR is responsible for the colour of the Au NPs/Alg–CA composite material. Formation of Au NPs was followed by observing absorption maxima at 540 nm with time (Fig. 3c). A plateau in the absorption maxima at 540 nm in around 5 hours supported the observation of visual colour change of Au NPs/Alg–CA. Furthermore, we have optimized the amount of $HAuCl_4$ for the composition of 3 wt% Alg and 0.5 M CA. A concentration

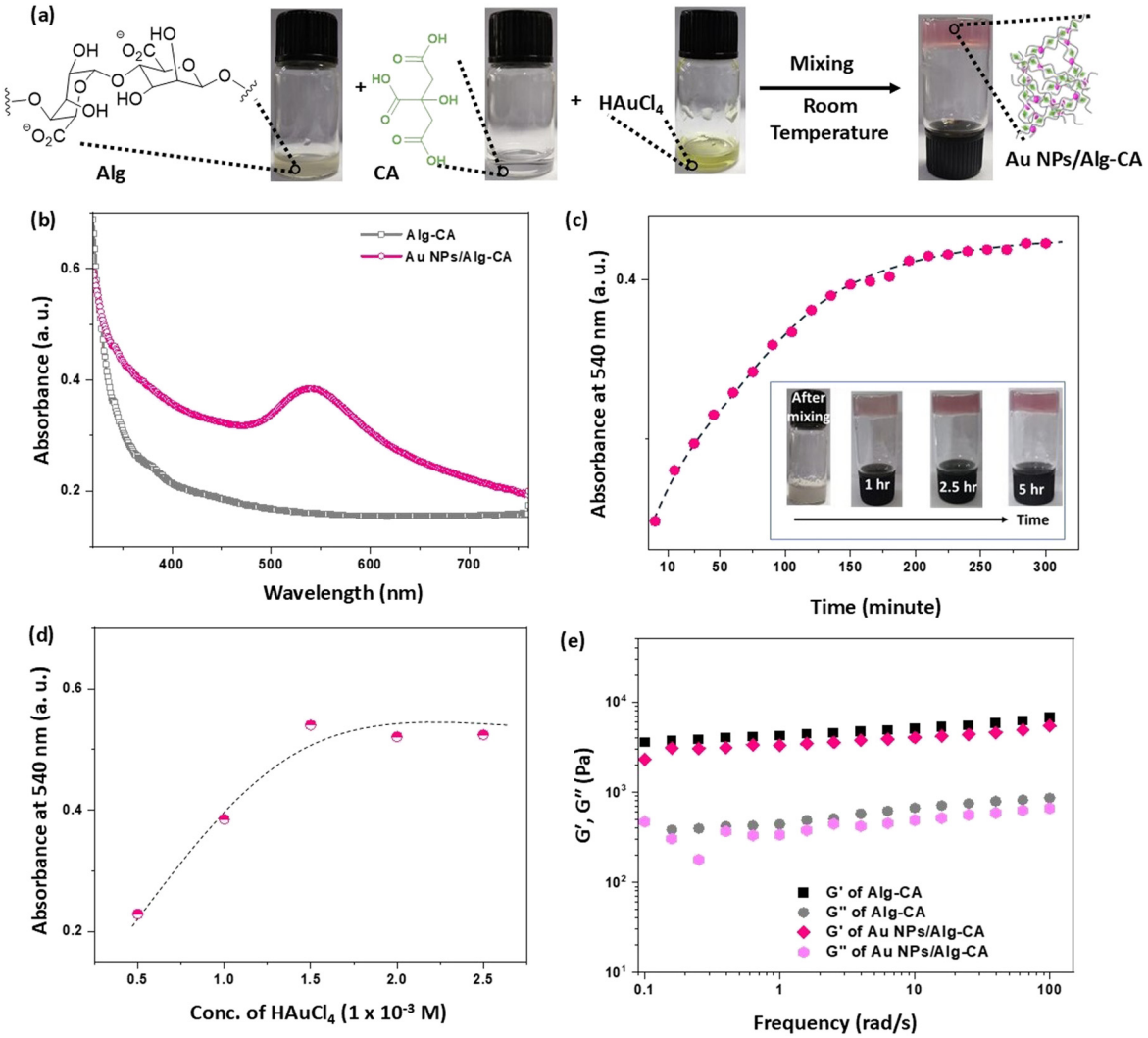

Fig. 3 *In situ* formation of Au NPs in Alg–CA. (a) A schematic for the preparation of Au NPs/Alg–CA *via* mixing aqueous solution of Alg, CA, and $HAuCl_4$ at room temperature. (b) Comparative UV-vis spectra of Au NPs/Alg–CA (pink line) and Alg–CA (grey line). (c) Evolution of Au NPs in the Alg–CA network with time (inset: appearance of the material at different times). The dotted line is drawn to guide the eyes. (d) The UV-vis spectrum of Au NPs/Alg–CA with different concentrations of $HAuCl_4$. The dotted line is drawn to guide the eyes. (e) Frequency sweep with 0.1% strain amplitude for rheological analysis of Alg–CA (*G*″, black squares; *G*′, grey circles) and Au NPs/Alg–CA (*G*″, pink diamonds; *G*′, magenta hexagons).

of 1.5×10^{-3} M was found to be the optimized concentration of $HAuCl_4$ for the preparation of Au NPs/Alg–CA as further increase in $HAuCl_4$ concentration did not provide the enhancement in the absorbance at 540 nm (Fig. 3d). It is worth noting that mixing $HAuCl_4$ and Alg alone yielded a yellowish solution after 24 h, while $HAuCl_4$ and CA provided a light pink, viscous solution after the same period in control experiments. However, formation of Au NPs within Alg–CA did not influence the hydrogel network as IR analysis of Au NPs/Alg–CA indicated no change in hydrogen bonding and ionic interactions (Fig. S3). Rheology measurement of Au NPs/Alg–CA suggested comparable viscoelastic properties to the Alg–CA hydrogel, indicating that the formation of Au NPs within the Alg–CA hydrogel network did not affect the strength of the material (Fig. 3e).

We recorded FESEM images for the morphological characterization of the Au NPs/Alg–CA material, showing a flower-like structure, which is comparable to the FESEM images of the Alg–CA material (Fig. 4a, and S4). The EDX spectrum was recorded to evaluate the elements present in

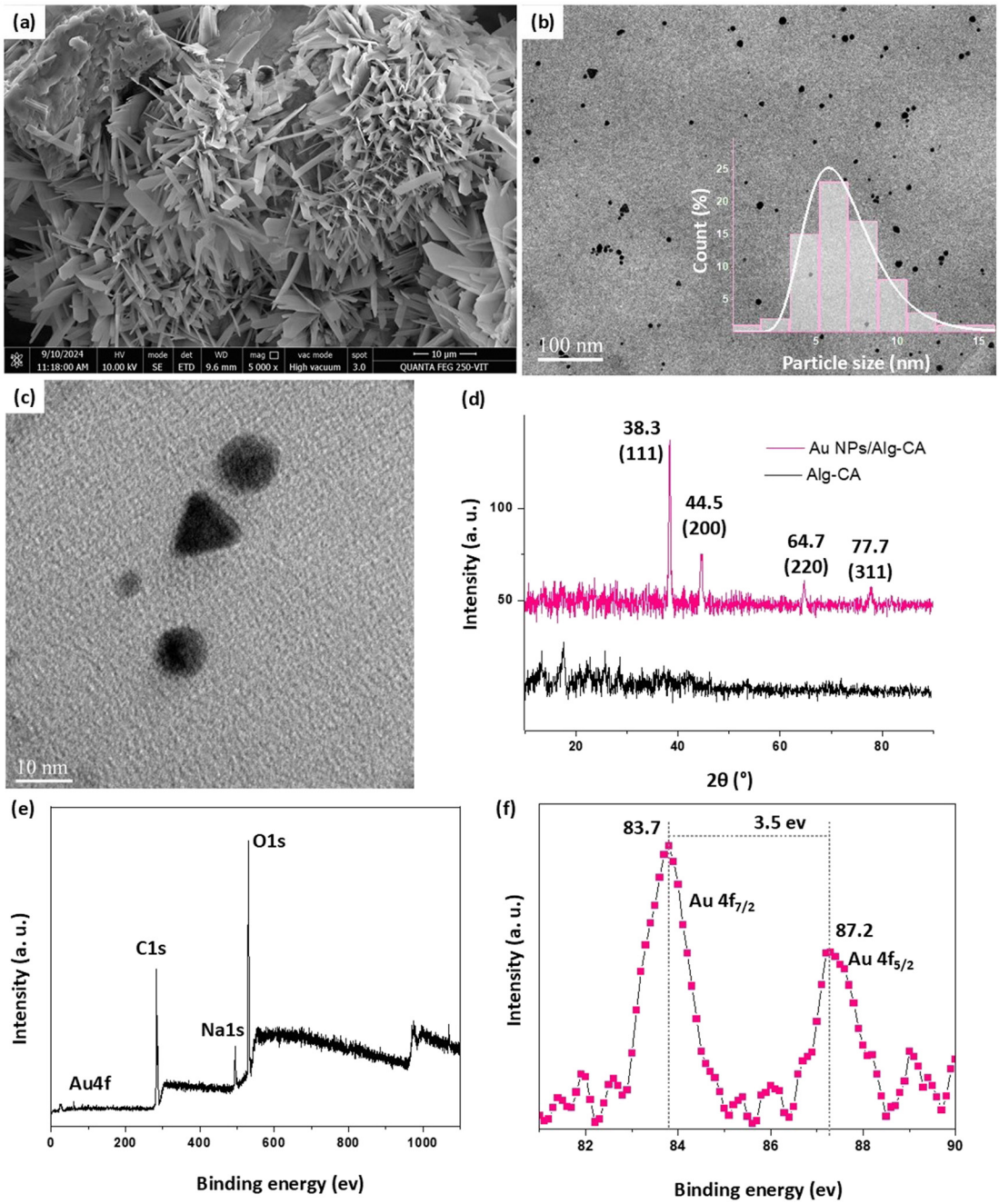

Fig. 4 Characterization of Au NPs/Alg–CA. (a) FESEM image of Au NPs/Alg–CA. (b) TEM image of the Au NPs/Alg–CA material (inset: size distribution histogram with Gaussian fitting). (c) High resolution TEM image showing circular and triangular-shaped Au NPs. (d) XRD patterns of Au NPs/Alg–CA (pink line) and Alg–CA (black line). (e) XPS pattern of Au NPs/Alg–CA. (f) High resolution XPS spectra of Au $4f_{7/2}$ and Au $4f_{5/2}$.

the material, confirming the presence of oxygen, carbon, sodium, and chlorine, alongside a detectable fraction of gold (Fig. S5). Besides, distribution of the gold element on the hydrogel material was mapped, showing even distribution (Fig. S6). Furthermore, we recorded the transmission electron micrograph (TEM) to determine the size distribution of Au NPs (Fig. 4b and S7). Spherical and triangular-shaped NPs were observed in the TEM images (Fig. 4c). Average particle size was analysed as ~6 nm (inset, Fig. 4b). It is worth mentioning that the average particle size was increased (6 nm → 10 nm) with increasing the concentration of $HAuCl_4$ (0.5×10^{-3} M → 1.0×10^{-3} M) (Fig. S8). Next, X-ray diffraction (XRD) patterns of Au NPs/Alg–CA were analysed and compared with Alg–CA. The spectrum for Alg–CA indicated an amorphous material (Fig. 4d, black line). In comparison, sharp diffraction peaks were observed for Au NPs/Alg–CA at 38.3°, 44.5°, 64.7° and 77.7°, which could be indexed to 111, 200, 220 and 311, respectively (Fig. 4d, pink line). This indicated the crystalline plane of the face-centred cubic structure of the metallic gold as reported by the Joint Committee on Powder Diffraction Standards (JCPDS) file no: 04-0784.[42,43] A high intense peak at 38.3° indicated the majority formation of Au NPs with the same orientation. The crystallite size as estimated by the Debye–Scherrer formula was 9.6 nm. Furthermore, X-ray photoelectron spectroscopy (XPS) analysis of Au NPs/Alg–CA showed three intense peaks located in the regions corresponding to O (530 eV), Na (496.4 eV), and C (283.6 eV) and one less intense peak located in the region corresponding to Au (Fig. 4e). The less intense peak is presumably due to the presence of a low percentage of Au compared to other elements. However, high-resolution XPS spectra for Au NPs showed two well-defined peaks centred at 83.7 eV and 87.2 eV with an energy separation of 3.5 eV (Fig. 4f), which corresponds to the $4f_{7/2}$ and $4f_{5/2}$ orbits of Au(0) in the nanoparticle core.[44,45] These results indicated that control formation of Au NPs within the Alg–CA network is feasible by mixing aqueous components under ambient conditions where hydrogel networks supported the formation of Au NPs and stabilized the Au NPs *via* preventing agglomeration.

4. Catalytic dye degradation application

Various anthropogenic activities including direct discharge of industrial contaminants in water bodies pose a serious risk to both environmental and human health, making rapid and effective removal of pollutants from wastewater essential. Among the diverse remediation strategies, catalytic degradation of organic dyes using Au NPs is an emerging approach due to their stability, excellent activity under ambient conditions, and environmentally benign nature.[46,47] However, the catalytic effectiveness of Au NPs is hindered by their tendency to aggregate, poor stability, low recycling ability, high cost and susceptibility to self-corrosion in aqueous media.[48,49] We envisioned that the use of the Au NPs/Alg–CA material would facilitate dye degradation in the presence of a reducing agent such as sodium borohydride ($NaBH_4$) and would allow the degradation for multiple cycles.

4.1. Congo red degradation

We examined the usability of the Au NPs/Alg–CA material for dye degradation application taking Congo red (CR) as a model dye molecule. CR, a benzidine-based anionic azo dye, is widely used in textile, leather, paper, and printing industries. However, it is considered as a major environmental pollutant due to its high stability and potential toxicity and carcinogenicity to humans and animals.[50,51] Therefore, it is important to remove CR from the industry effluents. We have employed the Au NPs/Alg–CA material in the presence of $NaBH_4$ for the degradation of CR in aqueous solution. A visual colour change was observed (red → colourless) after the treatment of CR solution (0.1 mM) with $NaBH_4$ (10 mM) and Au NPs/Alg–CA within 5 min (Fig. 5a). The decolouration was further monitored *via* UV-vis spectroscopy. The CR solution exhibited its characteristic peak at 500 nm, which progressively reduced within 5 minutes of treatment with Au NPs/Alg–CA and $NaBH_4$ (Fig. 5b and S9). In the control experiment, no complete decolourization was observed even after 60 minutes in the presence of only $NaBH_4$ or only Au NPs/Alg–CA. A pseudo-first-order kinetics (rate constant = 50.6×10^{-2} min^{-1}) was observed for CR solution decolouration in the presence of Au NPs/Alg–CA and $NaBH_4$, whereas the rate constants were comparatively low in the presence of only Au NPs/Alg–CA (rate constant = 0.23×10^{-2} min^{-1}) or in the presence of only $NaBH_4$ (rate constant = 0.30×10^{-2} min^{-1}). The decolouration efficiency for CR solution was calculated as 91.0% in 5 min *via* the treatment with Au NPs/Alg–CA and $NaBH_4$, whereas it was only 31.1% in 60 min *via* the treatment with only $NaBH_4$ and 21.0% in 60 minutes *via* the treatment with only Au NPs/Alg–CA. At higher CR concentrations (>0.1 mM), the degradation efficiency decreased, while 0.1 mM CR achieved 91% degradation within 5 min. Hence, 0.1 mM was selected for subsequent studies to ensure rapid and efficient degradation. For further confirmation of CR degradation, the colourless treated solution was analysed with MS spectroscopy. It showed the peaks at 184, 158, 128, and 316 m/z ratios (Fig. S10). The presence of only the lower mass fragmentation confirmed the degradation of CR dye presumably *via* breakdown of azo groups (plausible mechanism in Fig. S11).

Next, we set out for the recyclability test of the material as it is an important factor for assessing its practical performance.[52] For this, a solution of CR (0.1 mM in water) was mixed with $NaBH_4$ solution (10.0 mM in water) and the mixture was treated with Au NPs/Alg–CA (2.0 mL in a glass vial). After the colour change of the CR solution (red → colourless) within 5 min, the solution was filtered and the material was further treated with a fresh batch of CR solution and $NaBH_4$ solution. Reusability was analysed *via* UV-vis

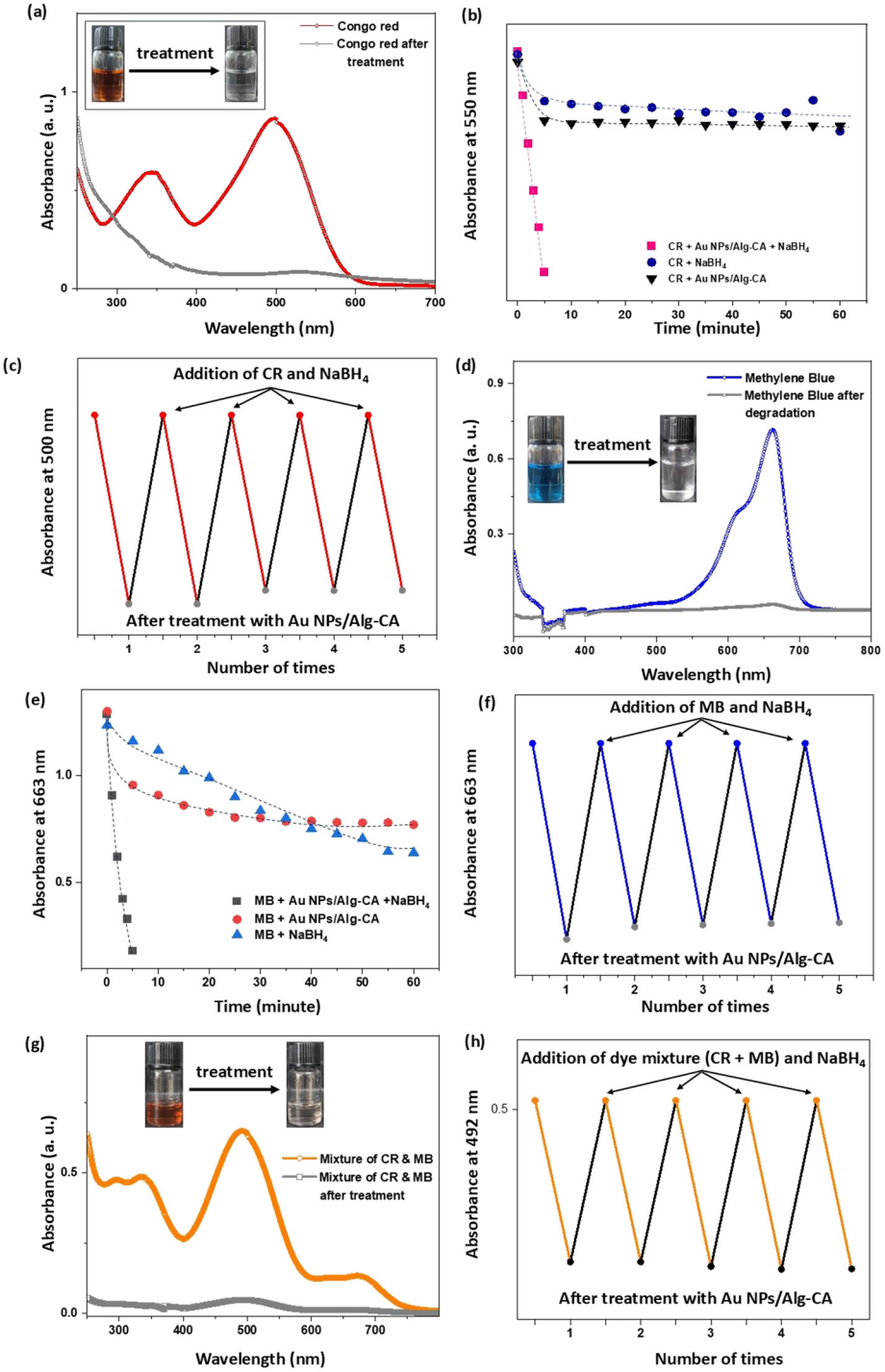

Fig. 5 Dye degradation with the Au NPs/Alg–CA composite material. (a) Optical absorbance spectra of CR solution before and after the treatment with Au NPs/Alg–CA and $NaBH_4$ (inset: the vial containing the CR solution before and after the treatment). (b) Relative rates of CR degradation in the presence of the Au NPs/Alg–CA material and $NaBH_4$ (pink squares), in the presence of only the Au NPs/Alg–CA material (black triangles), and in the presence of only $NaBH_4$ (blue circles). (c) Recyclability test of the material for CR degradation following the absorbance at 500 nm. (d) Optical absorbance spectra of the MB solution before and after the treatment with Au NPs/Alg–CA and $NaBH_4$ (inset: the vial containing the MB solution before and after the treatment). (e) Relative rates of MB degradation in the presence of the Au NPs/Alg–CA material and $NaBH_4$ (black squares), in the presence of only the Au NPs/Alg–CA material (red circles), and in the presence of only $NaBH_4$ (blue triangles). (f) Recyclability test of the composite material for MB solution following the absorbance at 663 nm. (g) Optical absorbance spectra of the dye mixture containing CR and MB dyes before and after the treatment with Au NPs/Alg–CA and $NaBH_4$ (inset: the vial containing the dye mixture before and after the treatment). (h) recyclability test of the composite for the mixture of CR and MB dyes following the absorbance at 492 nm. The lines are drawn to guide the eyes.

spectroscopy following the absorbance at 500 nm (Fig. 5c). It was observed that the material could be used up to 5 cycles (*vide infra*).

Quick decolouration of the dye solution in the presence of Au NPs/Alg–CA and $NaBH_4$ is plausibly due to the reduction of CR *via* electron transfer by Au NPs to CR (as an electron acceptor).[53] Adsorption of borohydride (BH_4^-) ions on the surface of Au NPs allowed electron transfer to the CR molecules. The large surface area of Au NPs resulted in efficient electron transfer and faster reduction of the dye molecules into lower-molecular-weight fragments, which subsequently desorb from the Au NP surface (Fig. S12).

4.2. Methylene blue degradation

Next, we applied a similar degradation approach for methylene blue (MB) dye as it is widely used in several applications as a cationic dye, and it has potential toxicity.[54] Degradation of MB solution (0.05 mM) was monitored *via* UV-vis spectroscopy. Decolouration was observed within 5 minutes after the treatment with Au NPs/Alg–CA in the presence of $NaBH_4$ (Fig. 5d). The decolourization efficiency was calculated as 97.5% (Fig. S13a and b). In contrast, no complete decolouration was observed even after 60 minutes in the presence of only Au NPs/Alg–CA (32.3% degradation efficiency) or only $NaBH_4$ (48.17% degradation efficiency). A pseudo-first-order kinetics (rate constant = 69.1×10^{-2} min^{-1}) was observed for MB decolouration when it was treated with Au NPs/Alg–CA and $NaBH_4$, whereas it was low (rate constant = 0.56×10^{-2} min^{-1} for only Au NPs/Alg–CA and rate constant = 1.14×10^{-2} min^{-1} for only $NaBH_4$) in control experiments. It is worth mentioning that a higher MB concentration (0.1 mM) resulted in 85% degradation within 5 min (k = 0.3811 min^{-1}), whereas 0.05 mM MB achieved 97.5% degradation in the same period (Fig. S13c). Therefore, the lower concentration was selected for subsequent studies to ensure rapid and efficient degradation. The MS spectrum of the degraded solution showed peaks at 227, 202, 158 and 122 m/z ratios (Fig. S14). The presence of different lower mass fragments for the colourless solution suggested the degradation of the MB dye *via* breakdown of the azo group (plausible mechanism in Fig. S15).

Being able to degrade the MB solution in a short time, we investigated the recycling ability of the Au NPs/Alg–CA material by treating a mixture of MB (0.05 mM in water) and $NaBH_4$ solution (10.0 mM in water) with Au NPs/Alg–CA (2.0 mL). After the decolouration of the MB solution (blue → colourless) in 5 min, the composite material was filtered and further treated with a fresh mixture of MB and $NaBH_4$. The reusability test was monitored using UV-vis spectroscopy following the absorbance at 663 nm (Fig. 5f). We observed that the material could be used for 5 cycles without compromising the efficiency. The material remained in the solution phase after 5 cycles as repeated addition of $NaBH_4$ increases the solution pH (basic pH of ~8), leading to decrosslinking of CA and deformation of the hydrogel network. FESEM images of the reused Au NPs/Alg–CA for 3 consecutive cycles confirmed the deformation in network morphology (Fig. S16). It is worth mentioning that the composite material exhibited superior efficiency for aqueous dye degradation compared to other reported similar systems under ambient conditions (Table S1),[55–58] highlighting its potential as an eco-friendly and effective alternative to conventional catalytic approaches.

4.3. Degradation of mixture of dyes

We further validated our dye treatment approach taking a mixed dye solution containing CR (0.05 mM) and MB (0.05 mM), reflecting typically found wastewater having multiple dyes.[59] We observed the usual colour change of the dye mixture (orange → colourless) in 10 minutes after the treatment with Au NPs/Alg–CA and $NaBH_4$. The optical absorbance of the mixture was followed *via* UV-vis spectroscopy, showing a change in absorption spectra in the visible region (Fig. 5g). Besides, the material could be reused 5 times without showing any change in activity (Fig. 5h). These results demonstrated the strong potential of the composite material for wastewater treatment under ambient conditions with multiple reusability.

4.4. Degradation of real textile wastewater

Textile wastewater samples were collected from a textile processing unit of Salem in Tamil Nadu, and transferred directly to the laboratory for investigating the degradation efficiency of the composite material. We treated the wastewater sample by mixing with Au NPs/Alg–CA and $NaBH_4$ under ambient conditions. A colour change of the wastewater (navy blue → colourless) was observed within 10 minutes, as confirmed by UV-vis spectroscopy monitoring the absorbance change (Fig. 6a). The material also showed a reusability of 5 times following absorbance at 600 nm (Fig. 6b). To gain further insight into the composition of the wastewater sample, high-resolution mass spectrometry (HRMS) analysis was performed (Fig. S17). The spectra exhibited prominent peaks at m/z 194, 453, 475, 608, and 744. Based on the characteristic navy-blue colour of the sample, these signals are most likely attributable to blue textile dyes, such as Reactive Blue 19 and/or a mixture of Reactive Blue 19 and Acid Blue 25, whose molecular weights correspond to the observed m/z values. This analysis supports the efficacy of the composite material in degrading a complex dye mixture.

We also analysed another textile wastewater sample that was collected post 'acid-wash treatment' from the textile industry to assess the degradation efficacy. Decolouration was observed in 10 minutes after treatment with Au NPs/Alg–CA and $NaBH_4$ that was confirmed by following optical absorbance in UV-vis spectroscopy (Fig. 6c). These results demonstrated the potential of the composite material to degrade industrial effluent under ambient conditions. Although employed in the gel phase for lab-scale experiments, industrial application would require process

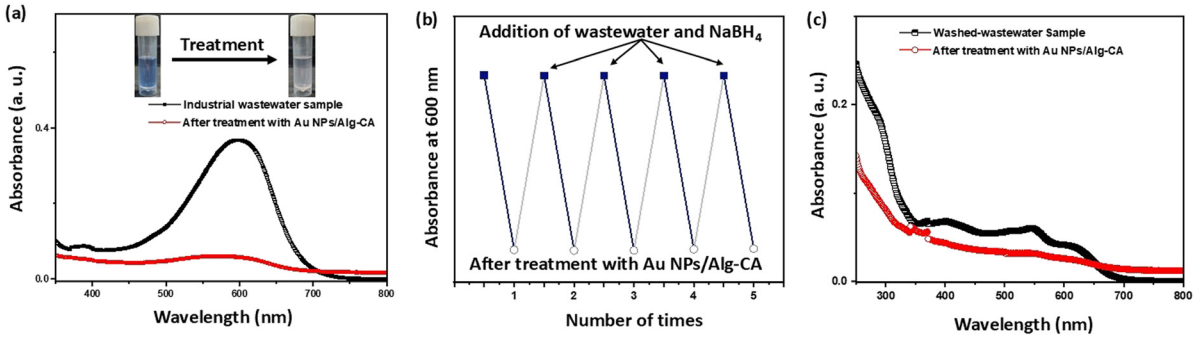

Fig. 6 Degradation of textile wastewater. (a) Optical absorbance spectra of the textile wastewater sample before (black line) and after (red line) the treatment with the composite material (inset: the vial containing wastewater before and after the treatment). (b) Recyclability test of the composite material for the wastewater sample following the absorbance at 600 nm. (c) Optical absorbance spectra of the wastewater sample containing textile dye after 'acid-wash' treatment.

adaptation to ensure practicality and reusability. At a larger scale, the hydrogel could be immobilized in columns for continuous-flow treatment in the presence of $NaBH_4$. However, practical implementation would necessitate optimization of $NaBH_4$ stability and release, gel mechanical strength, and catalyst regeneration cycles.

5. Antibacterial applications

Advanced antibacterial materials are crucial in biomedical applications mainly due to their effective inhibition of pathogenic microbes that are resistant towards antibiotics. We envisioned that Au NPs encapsulated in the Alg–CA hydrogel can offer an attractive strategy for the prevention and treatment of microbial infections as Au NPs can enhance the antimicrobial efficacy,[16] whereas the hydrogel can maintain controlled and sustainable delivery of the antimicrobial agent.

We first investigated the release of gold from Au NPs/Alg–CA within a simulated salivary fluid (pH 6.8) for 24 h. The concentration of gold was measured using atomic absorption spectrophotometry (AAS). Au NPs/Alg–CA was able to release 43% of Au NPs in 1 h and stabilized after 24 h with cumulative release. Next, the antimicrobial activity of the Au NPs/Alg–CA material was examined *via* a well diffusion method. Three infectious pathogenic bacteria, namely Gram-positive *Staphylococcus aureus* (*S. aureus*), Gram-negative *Escherichia coli* (*E. coli*), and *Acinetobacter baumannii* (*A. baumannii*), were used as model pathogens. A commonly used antibiotic compound (vancomycin against *S. aureus*, ciprofloxacin against *E. coli*, and chloramphenicol against *A. baumannii*) was used as a control for evaluating the zone of inhibition. Au NPs/Alg–CA exhibited larger inhibition zones across all bacterial pathogens in comparison to antibiotic molecules (Fig. 7a–c). Interestingly, *S. aureus* exhibited the highest susceptibility to Au NPs/Alg–CA with an inhibition zone of 27.6 ± 0.15 mm, followed by *A. baumannii* (19.0 ± 0.26 mm) and *E. coli* (17.0 ± 0.1 mm). In comparison to their respective standard antibiotics, the zone of inhibition was comparable in the case of *S. aureus* but significantly lesser than the antibiotics in the cases of *A. baumannii* and *E. coli.* The difference in zones of inhibition among bacteria is likely due to structural differences in bacterial cell walls. In comparison to Gram-negative bacteria, Gram-positive bacteria lack the outer lipopolysaccharide (LPS) membrane, making their peptidoglycan layer more accessible to Au NP-mediated interactions.[60] Additionally, the negative surface charge of the Au NPs (Table S2) may reduce the electrostatic interaction with the negatively charged bacterial cell surfaces. As bacterial cell walls generally carry a net negative charge,[61] Au NPs with a negative surface charge are less likely to bind effectively, thereby decreasing the antibacterial efficacy. However, only Alg–CA also demonstrated antimicrobial activity, albeit at a lesser extent to Au NPs/Alg–CA. This can be ascribed to the inherent antimicrobial properties of Alg and CA *via* modulating bacterial adhesion and biofilm formation.[62] Nevertheless, the enhanced antimicrobial inhibition by Au NPs/Alg–CA highlights the synergistic effect of Au NPs and the Alg–CA matrix. Besides, these results indicated the potent antimicrobial properties of the Au NPs/Alg–CA material presumably *via* disrupting bacterial membranes, generating reactive oxygen species (ROS), and interfering with the essential cellular functions. It is worth mentioning that the present study focuses on establishing the antibacterial efficacy of the material as a preliminary proof of concept. The hydrogel is envisioned primarily for potential external use applications, where localized delivery of antimicrobial agents is common, and no claims are made regarding its suitability for internal or systemic biomedical applications at this stage.

Next, we determined the minimum inhibitory concentration (MIC) of Au NPs/Alg–CA. The broth dilution assay provided the MIC of the formulated material against *S. aureus* (Fig. 7d), *E. coli* (Fig. 7e), and *A. baumannii* (Fig. 7f). The bacterial growth inhibition curve indicated a concentration-dependent response for both Au NPs/Alg–CA (red dots) and Alg–CA (orange dots) formulations. The MIC was found to be 0.5 mg mL^{-1} against *S. aureus*, *E. coli*, and *A. baumannii* with nearly complete inhibition (95.3% *S. aureus*, 91.6% *E. coli*, and 95.1% *A. baumannii*). However, Alg–CA alone exhibited a gradual decline in bacterial growth, suggesting limited intrinsic antimicrobial activity. The

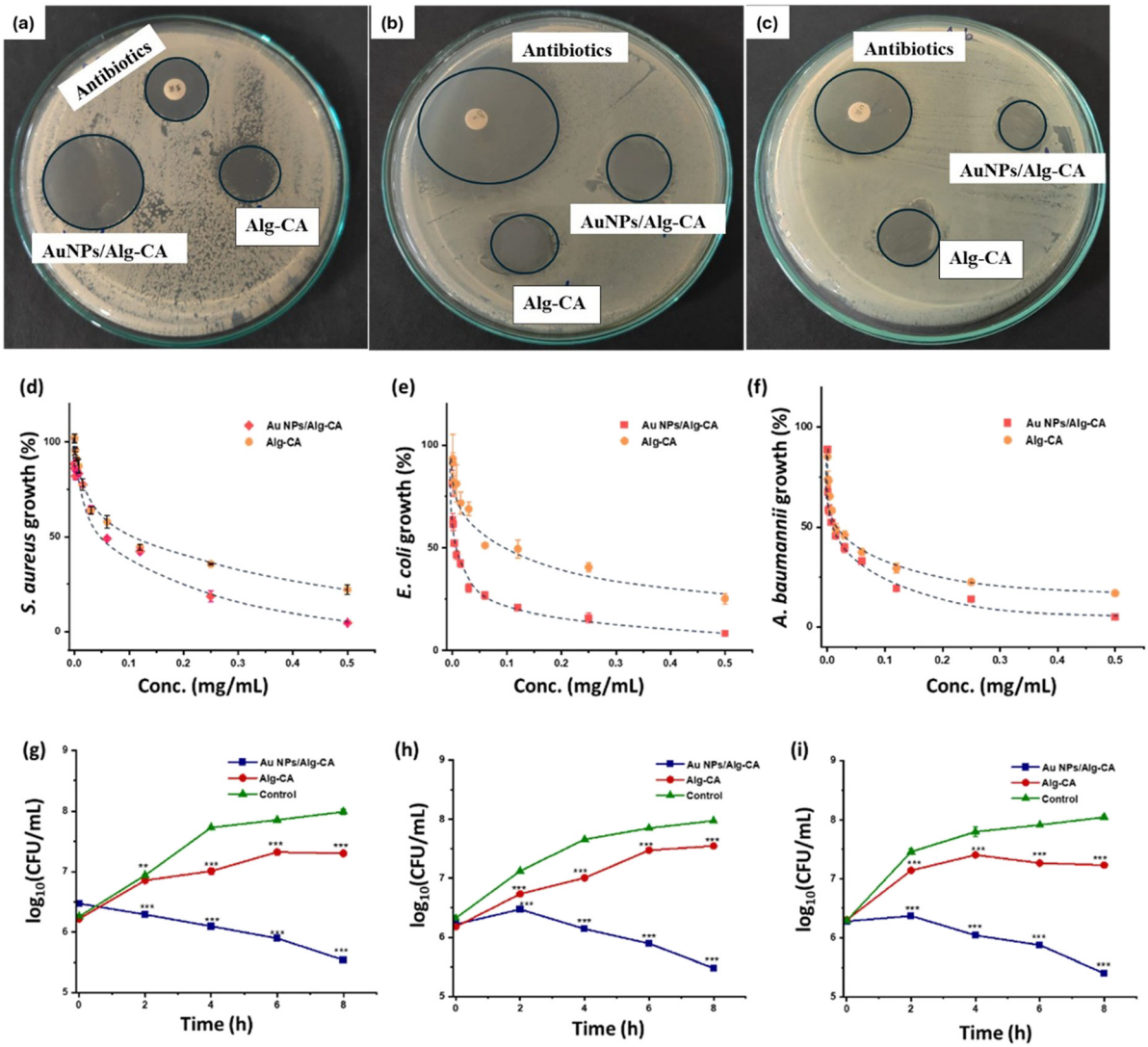

Fig. 7 Antibacterial activity of Au NPs/Alg–CA. (a–c) Zone of inhibition for the treatment of (a) *S. aureus* compared with Alg–CA and antibiotic vancomycin, (b) *E. coli* compared with Alg–CA and antibiotic ciprofloxacin, and (c) *A. baumannii* compared with Alg–CA and antibiotic chloramphenicol. (d–f) Minimum inhibitory concentration (MIC) determination for (d) *S. aureus* (red) compared to Alg–CA (yellow), (e) *E. coli* (red) compared to Alg–CA (yellow), and (f) *A. baumannii* (red) compared to Alg–CA (orange). (g–i) Time-kill kinetics of AuNPs/Alg–CA (blue line), Alg–CA (red line), and untreated control (green line) against (g) *S. aureus*, (h) *E. coli*, and (i) *A. baumannii* over an 8 hour period. Results are expressed as mean ± SD (n = 3); superscripts indicate a significant difference ($p < 0.001$) compared with the control group. The lines are drawn to guide the eyes.

enhanced bacterial inhibition observed with Au NPs/Alg–CA can be attributed to Au NP-induced membrane disruption and oxidative stress.[63]

Thereafter, a time-kill kinetics study was conducted over an 8 h period to evaluate the bactericidal effects of Au NPs/Alg–CA, Alg–CA, and control treatments against *S. aureus* (Fig. 7g), *E. coli* (Fig. 7h), and *A. baumannii* (Fig. 7i). A significant reduction in the bacterial count of *S. aureus* was observed in the group treated with Au NPs/Alg–CA, showing a progressive decline in $\log_{10}$ CFU mL^{-1} over time. In contrast, the Alg–CA and control groups showed increased bacterial growth, suggesting minimal to no bactericidal effect, whereas Au NPs/Alg–CA achieved a nearly 2-log reduction in 8 hours. This indicated the strong bactericidal activity of Au NPS/Alg–CA. Likewise, treatment with Au NPs/Alg–CA led to a notable decrease in *E. coli* and *A. baumannii* viability over time, while the Alg–CA and control groups showed logarithmic growth trends. The time-kill assay clearly demonstrated the enhanced antibacterial activity of Au NPs/Alg–CA compared to Alg–CA alone. The enhancement in the killing of resistant bacterial strains can be attributed to the synergistic effect of the Au NPs and the hydrogel matrix.[64]

To assess the antimicrobial potential of Au NPs/Alg–CA, MTT assays were performed against bacterial strains (*S. aureus*, *E. coli*, and *A. baumannii*), and viability was quantified following 24 hour exposure to different concentrations of Au NPs/Alg–CA and Alg–CA (ranging from 0.002 mg mL^{-1} to 0.5 mg mL^{-1}). MTT assays revealed that Au NPs/Alg–CA exhibited significantly enhanced

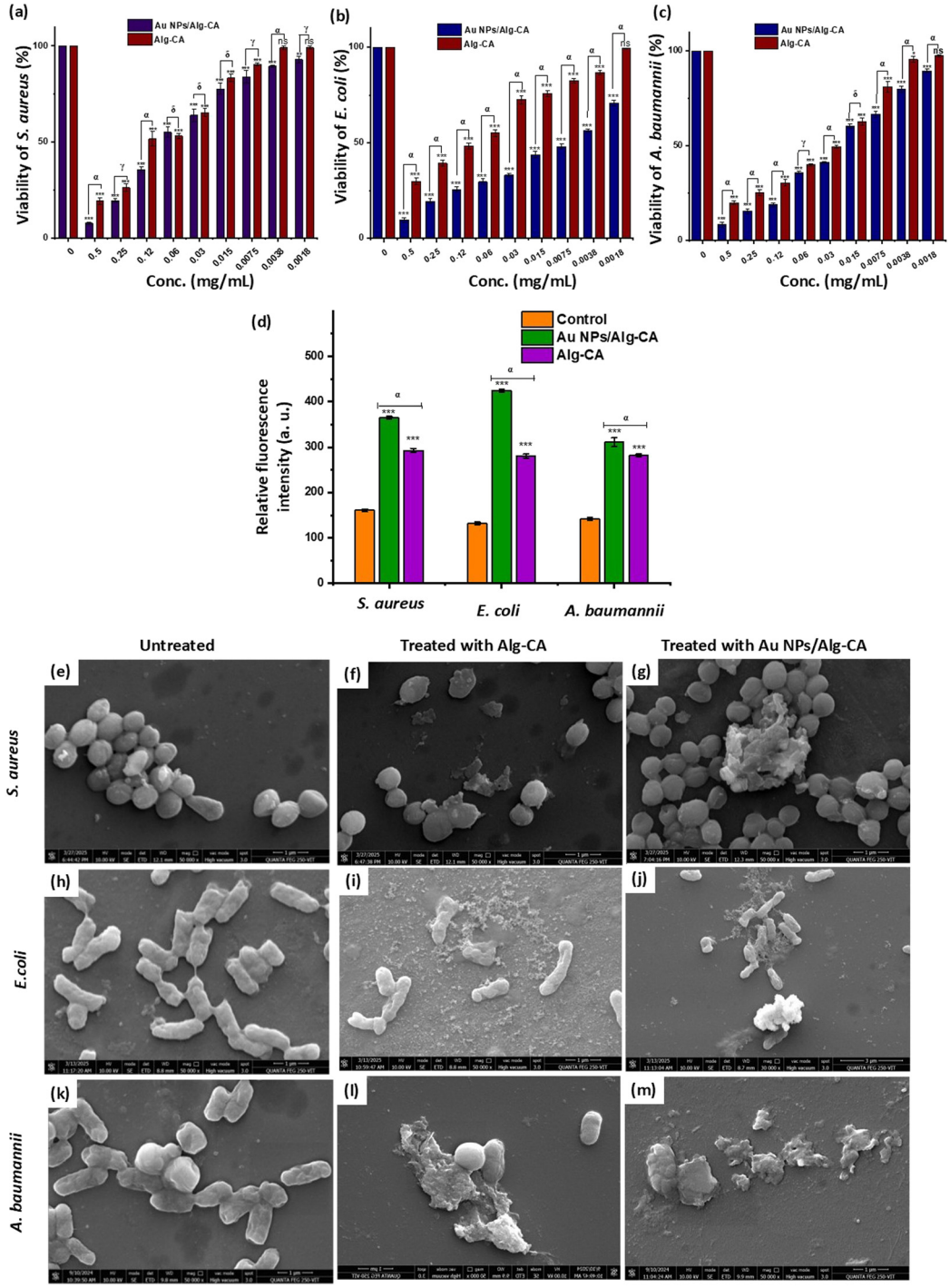

Fig. 8 (a–c) MTT assay for the testing of bacterial cell viability after the interaction with Au NPs/Alg–CA and Alg–CA: (a) *S. aureus*, (b) *E. coli*, and (c) *A. baumannii*. (d) Intracellular ROS levels in bacterial strains treated with Au NPs/Alg–CA and Alg–CA formulations. The level of significance for Au NPs/Ag-CA and Alg–CA compared with the control is marked with '***' ($p < 0.001$), 'α' indicates a significant difference between Au NPs/Alg–CA and Alg–CA ($\alpha = p < 0.001$). (e–m) FESEM images showing the morphology of the bacterial strains. (e–g) With *S. aureus*: (e) untreated, (f) treated with Alg–CA, and (g) treated with Au NPs/Alg–CA; (h–j) with *E. coli*: (h) untreated, (i) treated with Alg–CA, and (j) treated with Au NPs/Alg–CA; (k–m) with *A. baumannii*: (k) untreated, (l) Alg–CA, and (m) Au NPs/Alg–CA. Scale bar = 1 μm.

antimicrobial activity compared to Alg–CA alone (Fig. 8a–c). After 24 hour exposure, Au NPs/Alg–CA markedly reduced the bacterial viability in a dose-dependent manner, with the strongest effects observed at 0.5 mg mL^{-1}. *E. coli* showed the highest sensitivity, with the viability reduced to 9.64% ± 1.11 compared to 29.8% ± 1.74 for Alg–CA. This is presumably due to its thinner peptidoglycan layer facilitating nanoparticle penetration. Overall, Au NPs/Alg–CA

demonstrated superior bactericidal efficacy, especially against Gram-negative strains, highlighting the role of Au NPs in enhancing antimicrobial performance.

Exposure of bacterial cells to Au NPs may lead to a significant increase in reactive oxygen species (ROS) generation. Intracellular generation of ROS in *S. aureus*, *E. coli*, and *A. baumannii* was evaluated in the ROS assay exposing the bacterial cells to Au NPs/Alg–CA (Fig. 8d). The highest ROS production was observed for *S. aureus*, which was a 2.3-fold increase compared to the control experiment. A similar trend was observed for *E. coli* and *A. baumannii*. In contrast, the ROS levels were 2.5 times lower when only the Alg–CA matrix was used. These findings suggested that Au NPs actively contributed to the enhancement of oxidative stress in bacterial cells, resulting in ROS-mediated cellular damage. This can be attributed to the catalytic formation of $O_2^{\bullet-}$, $HO^{\bullet}$, or H_2O_2 by Au NPs that can disrupt bacterial cell membranes, denature proteins, and damage nucleic acids.[65] Additionally, the Alg–CA matrix allowed sustained release of Au NPs that facilitate ROS-mediated toxicity of the bacterial cells.

FESEM analysis was employed to observe the morphological changes in the bacterial cells after treatment with Au NPs/Alg–CA. The bacterial strains *S. aureus*, *E. coli* and *A. baumannii* were examined under the control (Fig. 8e, h and k), only Alg–CA (Fig. 8f, i and l), and Au NPs/Alg–CA (Fig. 8g, j and m) treated conditions. Untreated *S. aureus* cells appeared as spherical clusters with smooth surfaces (Fig. 8e). Some structural irregularities of a few cells were observed when treated with Alg–CA (Fig. 8f). In contrast, Au NPs/Alg–CA treatment caused substantial damage to the bacterial surface with clear ruptures and debris formation around the cells (Fig. 8g), confirming its enhanced antibacterial activity. Likewise, *E. coli* (Fig. 8h–j) and *A. baumannii* (Fig. 8m) maintained their typical rod-shaped morphology with smooth and intact surfaces under control conditions. Treatment with Alg–CA resulted in slight membrane deformation and reduced cell density. Treatment with Au NPs/Alg–CA caused significant morphological damage in *E. coli*, including cell shrinkage, membrane disruption, and, in some cases, complete lysis. The effects were more pronounced in *A. baumannii*, showing clear signs of cell aggregation, membrane collapse, and cell fragmentation. FESEM image analysis confirmed the severe structural damage in all tested bacterial strains *via* the treatment with Au NPs/Alg–CA. Besides, these results also indicated the antibacterial mechanism of Au NPs, where interactions with the bacterial membrane led to oxidative stress and disruption of cellular processes, resulting in cell death.[66]

6. Conclusions

In conclusion, we have developed a simple and efficient method for synthesizing Au NPs embedded in a biopolymer-based hydrogel matrix under ambient conditions. By mixing aqueous solution of sodium alginate (Alg), citric acid (CA), and gold salts such as $HAuCl_4$, Au NPs were formed *in situ* within the Alg–CA hydrogel matrix, where CA served both as a crosslinker and reducing agent. This approach allowed controlled growth of Au NPs within the hydrogel matrix at room temperature without addition of any exogenous agent and stabilizing agent or requirement of specific instrument support such as heat, light and ultrasound sources.

In situ prepared Au NPs embedded in the Alg–CA hydrogel matrix showed potential applications in environmental and biomedical applications. They efficiently degraded aqueous solutions of organic dyes such as Congo red and methylene blue within 5 minutes in the presence of $NaBH_4$ and retained its catalytic activity over multiple cycles. In addition to degrading individual organic dyes, the composite material demonstrated effective degradation of dye mixtures and textile industry wastewater, highlighting its potential for use in effluent treatment.

Furthermore, the material exhibited promising antibacterial activity by inhibiting the growth of pathogenic Gram-positive (*S. aureus*) and Gram-negative (*E. coli* and *A. baumannii*) bacteria through ROS-mediated membrane disruption. The hydrogel matrix also contributes by enabling the controlled release of antimicrobial agents. Although the antibacterial efficacy may be lower than that of conventional antibiotics, these materials present a key advantage in reducing the risk of resistance development. Future investigations are necessary to assess cytotoxicity, long-term biocompatibility, and the safety of all components to support potential biomedical applications.

These features suggest the significant potential of the prepared material for both in the biomedical field and in environmental remediation. This approach can be further employed to other biopolymers and (non)metallic nanoparticles, offering an accessible solution for combating environmental pollution and antimicrobial resistance, especially in resource-limited settings.

Author contributions

C. M. and D. J. conceived the idea. D. J. designed and performed the experiments. G. M. performed the antimicrobial experiments, and P. S. supervised the biological study. C. M. supervised the research and wrote the manuscript. All authors analysed the data, commented on the manuscript, and have given approval to the final version of the manuscript.

Conflicts of interest

A part of this work has been filed as Indian patent application (Application No.: 202541006381) with all the authors as inventors.

Data availability

The data supporting this article have been included as supporting information (SI). Supplementary information: SI detailing additional data for structural, morphological, and

compositional characterization, surface charge properties, nanoparticle size distribution, and catalytic performance of Alg–CA and Au NPs/Alg–CA nanocomposites, including degradation kinetics, proposed mechanisms for CR and MB dyes, recyclability studies, and comparative rate constant analysis. See DOI: https://doi.org/10.1039/d5en00722d.

Acknowledgements

C. M. acknowledges the funding from Vellore Institute of Technology as a seed grant (no. SG20240013). All authors acknowledge the help of the central instrumental facility of VIT Vellore to carry out the work. Authors also acknowledge VIT University for providing support toward the APC.

References

1 S. David, S. Kim, S. Oh and Y. H. Kahng, Advances in decorated mobile composites for adsorption and photocatalytic dye degradation: A comprehensive review, *J. Hazard. Mater. Adv.*, 2025, **18**, 100600, DOI: 10.1016/j.hazadv.2025.100600.

2 Y. Du, X. Xu, Q. Liu, L. Bai, K. Hang and D. Wang, Identification of organic pollutants with potential ecological and health risks in aquatic environments: progress and challenges, *Sci. Total Environ.*, 2022, **806**, 150691, DOI: 10.1016/j.scitotenv.2021.150691.

3 M. Ahmed, M. O. Mavukkandy, A. Giwa, M. Elektorowicz, E. Katsou, O. Khelifi, V. Naddeo and S. W. Hasan, Recent developments in hazardous pollutants removal from wastewater and water reuse within a circular economy, *npj Clean Water*, 2022, **5**, 12, DOI: 10.1038/s41545-022-00154-5.

4 Z. Zheng, J. He, Z. Zhang, A. Kumar, M. Khan, C. W. Lung and I. M. C. Lo, Magnetically recyclable nanophotocatalysts in photocatalysis-involving processes for organic pollutant removal from wastewater: current status and perspectives, *Environ. Sci.: Nano*, 2024, **11**, 1784, DOI: 10.1039/D3EN00906H.

5 S. Raghav, V. Chavda, A. Yadav, G. Mansi, J. Raghav, P. Jain and D. Kumar, Advanced MOF-based materials for adsorptive and photocatalytic removal of emerging organic pollutants from wastewater, *Appl. Mater. Today*, 2025, **46**, 102865, DOI: 10.1016/j.apmt.2025.102865.

6 S. Hameed, S. Sharif, M. Ovais and H. Xiong, Emerging trends and future challenges of advanced 2D nanomaterials for combating bacterial resistance, *Bioact. Mater.*, 2024, **38**, 225–257, DOI: 10.1016/j.bioactmat.2024.04.033.

7 D. A. Dik, J. F. Fisher and S. Mobashery, Cell-wall recycling of the gram-negative bacteria and the nexus to antibiotic resistance, *Chem. Rev.*, 2018, **118**, 5952–5984, DOI: 10.1021/acs.chemrev.8b00277.

8 A. Gupta, S. Mumtaz, C.-H. Li, I. Hussain and V. M. Rotello, Combatting antibiotic-resistant bacteria using nanomaterials, *Chem. Soc. Rev.*, 2019, **48**, 415–427, DOI: 10.1039/C7CS00748E.

9 A. J. Clasky, J. D. Watchorn, P. Z. Chen and F. X. Gu, From prevention to diagnosis and treatment: Biomedical applications of metal nanoparticle-hydrogel composites, *Acta Biomater.*, 2021, **122**, 1–25, DOI: 10.1016/j.actbio.2020.12.030.

10 W. Choi and D. S. Kohane, Hybrid nanoparticle–hydrogel systems for drug delivery depots and other biomedical applications, *ACS Nano*, 2024, **18**, 22780–22792, DOI: 10.1021/acsnano.4c06888.

11 J. Y. Lim, L. Goh, K. I. Otake, S. S. Goh, X. J. Loh and S. Kitagawa, Biomedically-relevant metal organic framework-hydrogel composites, *Biomater. Sci.*, 2023, **11**, 2661–2677, DOI: 10.1039/D2BM01906J.

12 N. Mamidi, F. F. De Silva, A. B. Vacas, J. A. Gutiérrez Gómez, N. Y. Montes Goo, D. R. Mendoza, R. L. Reis and S. C. Kundu, Multifaceted hydrogel scaffolds: Bridging the gap between biomedical needs and environmental sustainability, *Adv. Healthcare Mater.*, 2024, **13**, 2401195, DOI: 10.1002/adhm.202401195.

13 A. M. Gutierrez, E. M. Frazar, M. V. X. Klaus, P. Paul and J. Z. Hilt, Hydrogels and hydrogel nanocomposites: enhancing healthcare through human and environmental treatment, *Adv. Healthcare Mater.*, 2022, **11**, 2101820, DOI: 10.1002/adhm.202101820.

14 H. Song, D. H. Jung, Y. Cho, H. H. Cho, V. G. Panferov, J. Liu, J. H. Heo and J. H. Lee, Nanoparticle-integrated hydrogels as versatile colorimetric sensors, *Coord. Chem. Rev.*, 2025, **541**, 216835, DOI: 10.1016/j.ccr.2025.216835.

15 J. van Rie and W. Thielemans, Cellulose–gold nanoparticle hybrid materials, *Nanoscale*, 2017, **9**, 8525–8554, DOI: 10.1039/C7NR00400A.

16 A. Molinelli, A. Schirato, L. Moretti, G. D. Valle, M. Maiuri and F. Rossi, Last advances on hydrogel nanoparticles composites in medicine: an overview with focus on gold nanoparticles, *ChemNanoMat*, 2024, **10**, e202300584, DOI: 10.1002/cnma.202300584.

17 K. Xia, T. Yatabe, K. Yonesato, S. Kikkawa, S. Yamazoe, A. Nakata, R. Ishikawa, N. Shibata, Y. Ikuhara, K. Yamaguchi and K. Suzuki, Ultra-stable and highly reactive colloidal gold nanoparticle catalysts protected using multi-dentate metal oxide nanoclusters, *Nat. Commun.*, 2024, **15**, 851, DOI: 10.1038/s41467-024-45066-9.

18 P. Suchomel, L. Kvitek, R. Prucek, A. Panacek, A. Halder, S. Vajda and R. Zboril, Simple size-controlled synthesis of Au nanoparticles and their size-dependent catalytic activity, *Sci. Rep.*, 2018, **8**, 4589, DOI: 10.1038/s41598-018-22976-5.

19 Y. Guo, V. Walter, S. Vanuytsel, C. Parperis, J. T. Sengel, E. E. Weatherill and M. I. Wallace, Real-time monitoring and control of nanoparticle formation, *J. Am. Chem. Soc.*, 2023, **145**, 15809–15815, DOI: 10.1021/jacs.3c02484.

20 J. Perez-Juste, I. Pasteoriza-Santos, L. M. Liz-Marzán and P. Mulvaney, *Coord. Chem. Rev.*, 2005, **249**, 1870–1901, DOI: 10.1016/j.ccr.2012.09.002.

21 N. Sarfraz and I. Khan, Plasmonic gold nanoparticles (AuNPs): properties, synthesis and their advanced energy, environmental and biomedical applications, *Chem. – Asian J.*, 2021, **16**, 720–742, DOI: 10.1002/asia.202001202.

22 V. Jain, S. Roy, P. Roy and P. P. Pillai, When design meets function: the prodigious role of surface ligands in regulating nanoparticle chemistry, *Chem. Mater.*, 2022, **34**, 7579–7597, DOI: 10.1021/acs.chemmater.2c01941.

23 H. Duan, D. Wang and Y. Li, Green chemistry for nanoparticle synthesis, *Chem. Soc. Rev.*, 2015, **44**, 5778–5792, DOI: 10.1039/C4CS00363B.
24 V. Mehra, S. Kumar, A. M. Tamang and S. K. Chandraker, Green synthesis of gold nanoparticles (AuNPs) by using plant extract and their biological application: a review, *BioNanoSci.*, 2015, **15**, 18, DOI: 10.1007/s12668-024-01703-7.
25 N. Ahmad, S. N. A. Bukhari, M. A. Hussain, H. Ejaz, M. U. Munir and M. W. Amjad, Nanoparticles incorporated hydrogels for delivery of antimicrobial agents: developments and trends, *RSC Adv.*, 2024, **14**, 13535–13564, DOI: 10.1039/D4RA00631C.
26 Y. Qian, S. Lu, J. Meng, W. Chen and J. Li, Thermo-responsive hydrogels coupled with photothermal agents for biomedical applications, *Macromol. Biosci.*, 2023, **23**, 2300214, DOI: 10.1002/mabi.202300214.
27 A. Moreno and M. H. Sipponen, Overcoming challenges of lignin nanoparticles: expanding opportunities for scalable and multifunctional nanomaterials, *Acc. Chem. Res.*, 2024, **57**, 1918–1930, DOI: 10.1021/acs.accounts.4c00206.
28 X. Liu, S. Peng, Y. Pei, Y. Huo, Y. Zong, J. Ren and J. Zhao, Facile fabrication of chitosan/hyaluronic acid hydrogel-based wound closure material Co-loaded with gold nanoparticles and fibroblast growth factor to improve anti-microbial and healing efficiency in diabetic wound healing and nursing care, *Regener. Ther.*, 2024, **26**, 1018–1029, DOI: 10.1016/j.reth.2024.10.003.
29 G. A. Vinnacombe-Willson, M. Núñez-Martínez, A. Herrero-Ruiz, F. Bevilacqua, R. Pazos, L. Troncoso-Afonso, M. Gallego-González, L. Scarabelli and L. M. Liz-Marzán, Plasmonic-hydrogel hybrid biomaterials via in situ seeded growth, *Angew. Chem., Int. Ed.*, 2025, e202501854, DOI: 10.1002/anie.202501854.
30 V. V. Adole, G. Mishra and P. Chakraborty, Amyloid-inspired peptide hydrogels for in situ formation of catalytic nanoparticles: implications for environmental remediation, *ACS Appl. Nano Mater.*, 2025, **8**, 19535–19548, DOI: 10.1021/acsanm.5c03541.
31 P. Agnihotri and A. Dan, Temperature-and pH-responsive hydrogel nanoparticles with embedded Au nanoparticles as catalysts for the reduction of dyes, *ACS Appl. Nano Mater.*, 2022, **5**, 10504–10515, DOI: 10.1021/acsanm.2c01846.
32 D. Jagankar, N. Das, A. Mukherjee and C. Maity, Room-temperature synthesis of silver-based nanoparticle-embedded hydrogel material via catalytic crosslinking for recyclable dye degradation applications, *RSC Adv.*, 2025, **15**, 34068, DOI: 10.1039/d5ra03595c.
33 M. R. Marques, R. Loebenberg and M. Almukainzi, Simulated biological fluids with possible application in dissolution testing, *Dissolution Technol.*, 2011, **18**, 15–28, DOI: 10.14227/DT180311P15.
34 E. B. Adusei, R. K. Adosraku, J. Oppong-Kyekyeku, C. D. Amengor and Y. Jibira, Resistance modulation action, time-kill kinetics assay, and inhibition of biofilm formation effects of plumbagin from *Plumbago zeylanica Linn*, *J. Trop. Med.*, 2019, **1**, 1250645, DOI: 10.1111/j.1067-1927.2005.130409.x.
35 B. Das, S. K. Dash, D. Mandal, T. Ghosh, S. Chattopadhyay, S. Tripathy, S. Das, S. K. Dey, D. Das and S. Roy, Green synthesized silver nanoparticles destroy multidrug resistant bacteria via reactive oxygen species mediated membrane damage, *Arabian J. Chem.*, 2017, **10**, 862–876, DOI: 10.1016/j.arabjc.2015.08.008.
36 E. Grela, J. Kozłowska and A. Grabowiecka, Current methodology of MTT assay in bacteria–A review, *Acta Histochem.*, 2018, **120**, 303–311, DOI: 10.1016/j.acthis.2018.03.007.
37 M. M. Perez-Madrigal, J. Torras, J. Casanovas, M. Haring, C. Aleman and D. D. Díaz, Paradigm shift for preparing versatile M^{2+} free gels from unmodified sodium alginate, *Biomacromolecules*, 2017, **18**, 2967–2979, DOI: 10.1021/acs.biomac.7b00934.
38 H. Song, A. R. Jang, S. Lee and S. Y. Lee, Application of sodium alginate-based edible coating with citric acid to improve the safety and quality of fresh-cut melon (*Cucumis melo L.)* during cold storage, *Food Sci. Biotechnol.*, 2024, **33**, 1741–1750, DOI: 10.1007/s10068-023-01475-y.
39 C. Maity and N. Das, Alginate-Based Smart Materials and Their Application: Recent Advances and Perspectives, *Top. Curr. Chem.*, 2022, **380**, 3, DOI: 10.1007/s41061-021-00360-8.
40 S. Paul, K. Basu, K. S. Das and A. Banerjee, Peptide-based hydrogels as a scaffold for in situ synthesis of metal nanoparticles: catalytic activity of the nanohybrid system, *ChemNanoMat*, 2018, **4**, 882–887, DOI: 10.1002/cnma.201800227.
41 A. K. Tamo, Nanocellulose-based hydrogels as versatile materials with interesting functional properties for tissue engineering applications, *J. Mater. Chem. B*, 2024, **12**, 7692–7759, DOI: 10.1039/D4TB00397G.
42 T. Jayaramudu, G. M. Raghavendra, K. Varaprasad, R. Sadiku and K. M. Raju, Development of novel biodegradable Au nanocomposite hydrogels based on wheat: for inactivation of bacteria, *Carbohydr. Polym.*, 2013, **92**, 2193–2200, DOI: 10.1016/j.carbpol.2012.12.006.
43 K. Jankowski, J. Jablonska, P. Uznanski, S. Caluch, M. Szybowicz, R. Brzozowski, A. Ostafin, M. Kwasny and M. Tomasik, Necked gold nanoparticles prepared by submerged alternating current arc discharge in water, *RSC Adv.*, 2022, **12**, 33955–33963, DOI: 10.1039/D2RA06050G.
44 S. Caporali, F. Muniz-Miranda, A. Pedone and M. Muniz-Miranda, SERS, XPS and DFT Study of xanthine adsorbed on citrate-stabilized gold nanoparticles, *Sensors*, 2019, **19**, 2700, DOI: 10.3390/s19122700.
45 P. Hepperle, A. Herman, B. Khanbabaee, W. Y. Baek, H. Nettelbeck and H. Rabus, XPS examination of the chemical composition of PEGMUA-coated gold nanoparticles, *Part. Part. Syst. Charact.*, 2022, **39**, 2200070, DOI: 10.1002/ppsc.202200070.
46 A. I. Osman, Y. Zhang, M. Farghali, A. K. Rashwan, A. S. Eltaweil, E. M. A. El-Monaem, I. M. A. Mohamed, M. M. Badr, I. Ihara, D. W. Rooney and P.-S. Yap, Synthesis of green nanoparticles for energy, biomedical, environmental, agricultural, and food applications: A review, *Environ. Chem. Lett.*, 2024, **22**, 841–887, DOI: 10.1007/s10311-023-01682-3.

47 A. Gellé, T. Jin, L. de la Garza, G. D. Price, L. V. Besteiro and A. Moores, Applications of plasmon-enhanced nanocatalysis to organic transformations, *Chem. Rev.*, 2020, **120**, 986–1041, DOI: 10.1021/acs.chemrev.9b00187.

48 M. Sankar, Q. He, R. V. Engel, M. A. Sainna, A. J. Logsdail, A. Roldan, D. J. Willock, N. Agarwal, C. J. Kiely and G. J. Hutchings, Role of the support in gold-containing nanoparticles as heterogeneous catalysts, *Chem. Rev.*, 2020, **120**(8), 3890–3938, DOI: 10.1021/acs.chemrev.9b00662.

49 K. Wang, J. Zhao, X. Zhang, L. Jiang, X. Zhou, C. Xie, X. Jia, L. Zhang and Z. Wu, Fluorescent noncovalent organic framework for supporting gold nanoparticles as heterogeneous catalyst with merits of easy detection and recycle, *Small*, 2024, **20**, 2303834, DOI: 10.1002/smll.202303834.

50 P. O. Oladoye, O. M. Bamigboye, O. D. Ogunbiyi and M. T. Akano, Toxicity and decontamination strategies of Congo red dye, *Groundw. Sustain. Dev.*, 2022, **19**, 100844, DOI: 10.1016/j.gsd.2022.100844.

51 S. Siddiqui, E. S. Allehyani, S. A. Al-Harbi, Z. Hasan, M. A. Abomuti, H. K. Rajor and S. Oh, Investigation of Congo red toxicity towards different living organisms: a review, *Processes*, 2023, **11**, 807, DOI: 10.3390/pr11030807.

52 A. Nyabadza, M. Makhesana, A. Plouze, A. Kumar, I. Ramirez, S. Krishnamurthy, M. Vazquez and D. Brabazon, Advanced nanomaterials and dendrimers in water treatment and the recycling of nanomaterials: a review, *J. Environ. Chem. Eng.*, 2024, **12**, 112643, DOI: 10.1016/j.jece.2024.112643.

53 G. K. Deokar and A. G. Ingale, Exploring effective catalytic degradation of organic pollutant dyes using environment benign, green engineered gold nanoparticles, *Inorg. Chem. Commun.*, 2023, **151**, 110649, DOI: 10.1016/j.inoche.2023.110649.

54 P. O. Oladoye, T. O. Ajiboye, E. O. Omotola and O. J. Oyewola, Methylene blue dye: toxicity and potential elimination technology from wastewater, *Results Eng.*, 2022, **16**, 100678, DOI: 10.1016/j.rineng.2022.100678.

55 N. Y. Nadaf and S. S. Kanase, Biosynthesis of gold nanoparticles by *Bacillus marisflavi* and its potential in catalytic dye degradation, *Arabian J. Chem.*, 2019, **12**, 4806–4814, DOI: 10.1016/j.arabjc.2016.09.020.

56 A. Haleem, S. Chen, J. Pan and H. Weidong, Gamma radiation induced synthesis of double network hydrophilic cryogels at low pH loaded with AuNPs for fast and efficient degradation of Congo red, *J. Hazard. Mater. Adv.*, 2023, **10**, 100299, DOI: 10.1016/j.hazadv.2023.100299.

57 K. B. Narayanan and H. H. Park, Homogeneous catalytic activity of gold nanoparticles synthesized using turnip (*Brassica rapa L.*) leaf extract in the reductive degradation of cationic azo dye, *Korean J. Chem. Eng.*, 2015, **32**, 1273–1277, DOI: 10.1007/s11814-014-0321-y.

58 B. R. Ganapuram, M. Alle, R. Dadigala, A. Dasari, V. Maragoni and V. Guttena, Catalytic reduction of methylene blue and Congo red dyes using green synthesized gold nanoparticles capped by *salmalia malabarica* gum, *Int. Nano Lett.*, 2015, **5**, 215–222, DOI: 10.1007/s40089-015-0158-3.

59 D. A. Yaseen and M. Scholz, Textile dye wastewater characteristics and constituents of synthetic effluents: a critical review, *Int. J. Environ. Sci. Technol.*, 2019, **16**, 1193, DOI: 10.1007/s13762-018-2130-z.

60 Y. N. Slavin, J. Asnis and U. O. Häfeli, Metal nanoparticles: understanding the mechanisms behind antibacterial activity, *J. Nanobiotechnol.*, 2017, **15**, 65, DOI: 10.1186/s12951-017-0308-z.

61 A. Girma, G. Mebratie, B. Mekuye, B. Abera, T. Bekele and G. Alamnie, Antibacterial capabilities of metallic nanoparticles and influencing factors, *Nano Sel.*, 2024, **5**, e202400049, DOI: 10.1002/nano.202400049.

62 L. C. Powell, M. F. Pritchard, E. L. Ferguson, K. A. Powell, S. U. Patel, P. D. Rye, S. Sakellakou, N. J. Buurma, C. D. Brilliant, J. M. Copping, G. E. Menzies, P. D. Lewis, K. E. Hill and D. W. Thomas, Targeted disruption of the extracellular polymeric network of Pseudomonas aeruginosa biofilms by alginate oligosaccharides, *npj Biofilms Microbiomes*, 2018, **4**, 13, DOI: 10.1038/s41522-018-0056-3.

63 H. Jiang, L. Li, Z. Li and X. Chu, Metal-based nanoparticles in antibacterial application in biomedical field: Current development and potential mechanisms, *Biomed. Microdevices*, 2024, **26**, 12, DOI: 10.1007/s10544-023-00686-8.

64 H. Meng, Y. Zhao, H. Cai, D. You, Y. Wang, S. Wu, Y. Wang, W. Guo and W. Qu, Hydrogels containing chitosan-modified gold nanoparticles show significant efficacy in healing diabetic wounds infected with antibiotic-resistant bacteria, *Int. J. Nanomed.*, 2024, **19**, 1539–1556, DOI: 10.2147/IJN.S448282.

65 K. Umamaheswari, R. Baskar, K. Chandru, N. Rajendiran and S. Chandirasekar, Antibacterial activity of gold nanoparticles and their toxicity assessment, *BMC Infect. Dis.*, 2014, **14**, 64, DOI: 10.1186/1471-2334-14-S3-P64.

66 Z. Batool, G. Muhammad and M. M. Iqbal, Hydrogel assisted synthesis of gold nanoparticles with enhanced microbicidal and in vivo wound healing potential, *Sci. Rep.*, 2022, **12**, 6575, DOI: 10.1038/s41598-022-10495-3.